White Paper XXVI

Tools for Understanding Both the Coarse and the Fine Levels of Physical Reality on Our Spiritual Journey Home

by

William A Tiller, PhD

Introduction

As we reflect upon our world and upon the humankind that populate its surface, one soon perceives that there are several categories of phenomena, energies and information wherein we need to gain reliable understanding in order to understand our life's journey. These might be classified as (1) things of the physical, (2) things of the psyche, (3) things of emotion, (4) things of the mind and (5) things of the spirit. In addition, we need a meaningful perspective or reference frame (RF) from which to view these different categories of entities. Ultimately, our understanding of all these various phenomena must be internally self-consistent with each other. Since we are an evolving species, growing in understanding via a bootstrap process, a useful metaphor for what we need is a "ladder of understanding" that guides us from the simple to the more complex.

Figure 1. A metaphorical description of "the ladder of understanding".

Thus, Figure 1 represents our metaphorical "ladder of understanding" (LOU) that we must carefully build by our collective efforts and then climb upon, rung by rung, to higher states of being. Let us look at where we stand today with respect to our LOU.

Orthodox science, and thus also orthodox medicine, has labored mightily for the past 400 years to build **the bottommost rung of the LOU**. They presently hold two major beliefs:

1. Mathematically, all true science findings must be internally self-consistent with each other via a distance-time-only RF (reference frame) and
2. No human qualities of consciousness, intention, emotion, mind or spirit can significantly influence a well-designed target experiment in physical reality (first posited by Descartes in ~1600 AD. This assumption has only recently been seriously tested, yet is still unconsciously held by most orthodox scientists and orthodox medical practitioners today).

These dictums led to the industrial revolution, with its explosion of new technology plus many forms of classical mechanics. A few of the major accomplishments of the past century are:

(a) Discovering and quantitatively certifying the existence of four fundamental forces operating in nature – gravity, electromagnetism, the long range nuclear force and the short range nuclear force,
(b) Quantum mechanics ($E = h\nu$) (QM)
(c) Relativistic mechanics ($E = mc^2$ & $v \leq c$)
(d) DeBroglie's particle/wave duality concept ($\lambda = h/p$; $\nu = E/h$)
(e) Dirac's concept of positive mass particle/antiparticle pair creation from a sea of negative energy states in the coarse physical vacuum
(f) Invisible gravitational attractors: Dark matter + Dark energy
(g) h = Planck's constant, m=mass, c=velocity of light in coarse physical vacuum, λ-wavelength, p=momentum and E=energy.
(h) Etc.

However, there appear to be a variety of **serious problems** with our present-day orthodox science paradigm. Let us look at some of them:

A. ~150 years of serious experimental observations of **anomalous** human cognition and **anomalous** human forces have been found to be **not** internally self-consistent with orthodox science belief #1 – and thus have been conveniently **ignored** and "swept under the rug" by the orthodox science & medicine community.
B. About a decade ago, orthodox belief #2 was seriously tested via four carefully designed and different target experiments plus four different, specific intentions, one for each target experiment, imprinted into an IHD (intention host device) and placed about a foot away from its continuously running companion target experiment. The experimental results of these four experiments[(1)] were robustly successful in proving that, in today's world, orthodox belief #2 is very, very wrong!

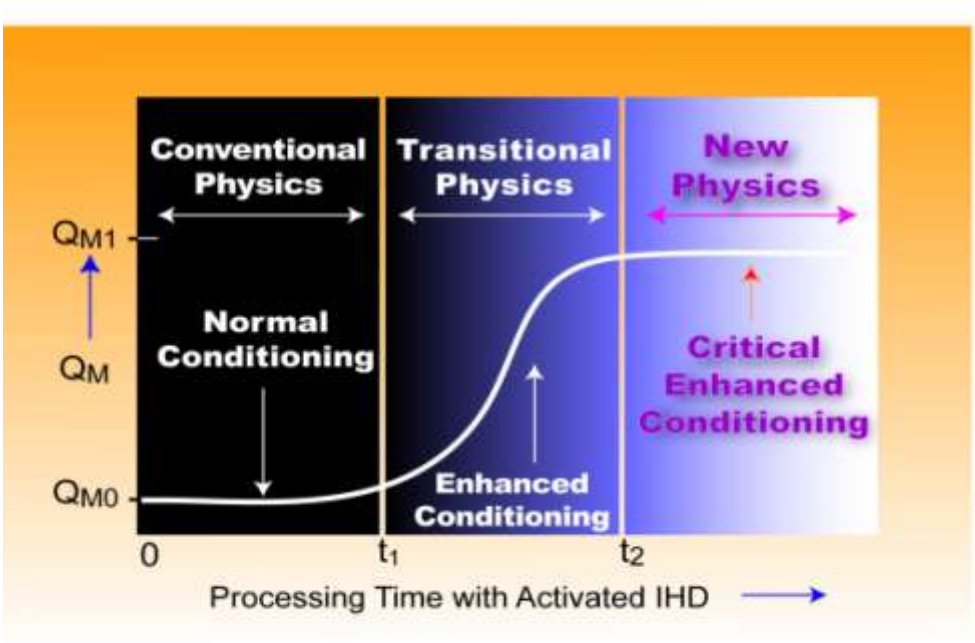

Figure 2. For any typical physical measurement, Q, the qualitative measureable magnitude change, Q_M, is plotted versus the degree of locale conditioning produced by continued IHD use.

Figure 2 illustrates that, for any typical IHD experiment, the qualitative magnitude of a specific material property change, Q_M, varies non-linearly with IHD-processing time from our ordinary electric atom/molecule value, Q_{M_o}, towards our IHD-determined value, Q_{M_1} (always in the proper direction but not always to Q_{M_1} if one removes the IHD from the experimental space before time, t_2, has been reached. In such a case, Q_M, just decays slowly back to Q_{M_o}. A simple zeroth-order approximation equation for representing Figure 2 is

$$Q_M(t) = Q_e + \alpha_{eff}(t)\, Q_m. \qquad (1)$$

Here, Q_e is our coarse physical reality (electric atom/molecule) value, Q_m is the imprinted, coarse physical vacuum (magnetic information wave) level and $\alpha_{eff}(t)$ is the time-varying coupling coefficient that allows these two very different media to interact with each other. If $\alpha_{eff}(t)$ slowly decays to zero then the second term disappears and our normal coarse physical reality is restored.

C. The two key cornerstones of QM are (1) Max Planck's experimental and theoretical observations that electromagnetic (EM) radiation emission and absorption by physical matter was in discrete-sized bits (quanta) rather than in continuously variable-sized bits and (2) DeBroglie's particle-pilot wave concept wherein both particles with mass or particles without mass (photons) have

associated with them **a pilot wave** that guides them during their travels. Harrison[(2)] has shown that all the rest of the QM formalism can be generated provided one assumes the **simultaneous** existence of physical matter as **both** a particle and a wave. Thus, we need to look at this concept of DeBroglie's very carefully.

We see the waves drawn in textbooks as continuous undulations without atomic graininess. However, all the waves cognitively accessed by human sense organs are all modulations of particle densities (water, air) and particle flux densities (light, sound). Nonetheless, when we consider the textbook example of a group of waves moving in the x-direction as in Figure 3, the entire group of wavelets propagates with velocity, v group (v_g), while the individual wavelets propagate with phase velocity, v.

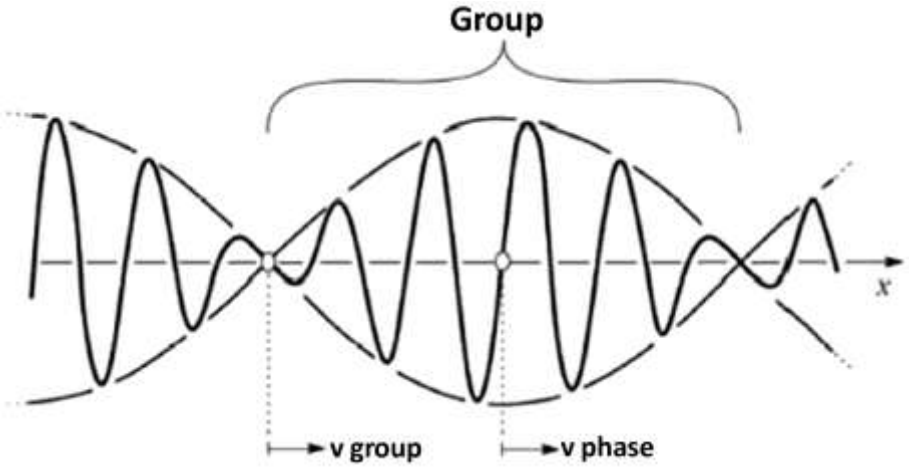

Figure 3. Example of a group of waves moving along the x-direction. The entire group of wavelets propagates with group velocity v_{group}. Individual wavelets propagate with phase velocity v_{phase}.

Here, v can be smaller than, equal to, or larger than v_g. In the latter case, $v > v_g$, the high frequency waves enter the group from the rear and exit the group from the front. In the opposite case that $v < v_g$, the direction of relative movement is reversed, a key experimental property governing the details of wave propagation in a particular medium is whether or not the wave is energetically interacting with the medium. If it is, then the medium is said to be a **dispersive** medium and $v \neq v_g$. For **non-dispersive** media, v is independent of the frequency of the wave and

$$v = v_g = \frac{w}{k} \qquad (2)$$

where $w = 2\pi\nu$, is the angular frequency of the wave (ν is its frequency) and $k = 2\pi/\lambda$ is its wave number (λ is its wavelength).

For water, if one throws a stone into a pond, the curves of constant phase emanating from the impact site are concentric circles with $v/v_g \sim 2$, so water is a somewhat dispersive medium.

Theoretically, DeBroglie postulated that the wavelength, λ, and frequency, ν, of the pilot waves associated with a particle of momentum p and total relativistic energy, E, are given by

$$\lambda = h/p \quad \text{and} \quad \nu = E/h \tag{3}$$

where Planck's constant ($\hbar = h/2\pi$). When one analyzes a group of waves (w,k) and a particle moving in one-dimension, for the non-relativistic particle energy case of $E = p^2/2m$, the math leads only to $v_g = v$. However, when one uses the relativistic energy where

$$E_R = [c^2p^2 + (m_oc^2)^2]^{1/2} = c[p^2 + (m_oc)^2]^{1/2}, \tag{4}$$

one finds that both

$$v_g = v_p \text{ and } w = c^2 / v_p\,, \tag{5}$$

Where w is the pilot wave velocity[3]. Since $v_p < c$, always, $w > c$, always. This can be readily seen from Equations 4 and 3 because

$$w = \lambda v = \frac{h}{p}\cdot\frac{E_R}{h} = \frac{E_R}{p} > c \tag{6}$$

for the non-dispersive case. This pilot wave cannot be experimentally observed via today's orthodox instruments which are limited by v = c.

Today's orthodox scientists are not particularly happy with Equation 5[4] because it violates the relativistic prediction that mass cannot travel faster than c. They prefer to propose that an absorption of the wave resulting from its dispersion nature changes the picture and solves the dilemma. However, when one looks at Equations 6 and 4, which doesn't involve wave dispersion properties, their proposal doesn't seem very reliable.

Taking the w > c position as viable would explain why the physical vacuum appears to be transparent to both today's optical instruments and to average human eyesight.

D. Today's orthodox science states that it doesn't understand (i) the nature of dark matter & dark energy, (ii) the nature of planet and star acceleration vs. deceleration at the outer edge of the cosmos and (iii) why the matter/antimatter ratio is found to be experimentally greater than unity.

To understand how one might explain these three important pieces of data, one needs only to seriously look at Figure 4 (from Dirac in the early 1930's).

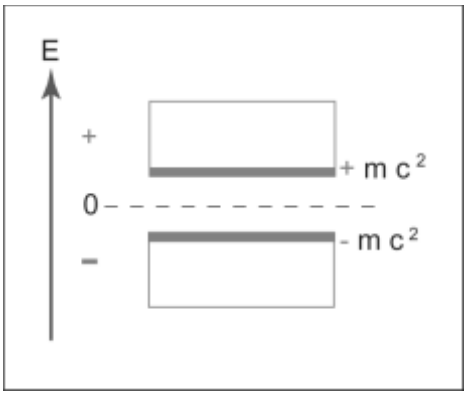

Figure 4. Schematic energy spectrum associated with the Dirac analysis. A band gap of forbidden energies exists between E = ±mc^2 for particle-antiparticle creation of mass 2m.

He was the first to ask the important question "where does an electron come from?" and the model he started with was the simplest of energy band diagrams. In Figure 4, the lower region is the coarse physical vacuum. Above this region is postulated to be a band-gap of theoretically disallowed energy states while, above that is a zone of allowed positive energy states, where electrons and other members of the physical particle community can exist. He utilized the quantitative mathematical formalism of relativistic quantum mechanics for his calculations

$$E = \pm[c^2p^2 + (m_oc^2)^2]^{1/2}\,, \qquad (7)$$

where m_o is the rest mass of the particle, p is its momentum and c is the velocity of EM light in a vacuum.

He postulated that a cosmic ray (a very high energy photon) traveling through this coarse physical vacuum could interact with this vacuum "stuff" and kick out something that becomes an electron in the positive energy region and leaves behind a positive energy "hole" in the negative energy region. Since the electron has a negative charge, for charge neutrality, the hole must have a positive charge of the same magnitude. Also, the positive energy hole was located in a zone of negative energy states so it acquired the same positive mass as the ejected electron. This hole was labeled the **positron** and became the very first anti-matter to be discovered. Over the following decades, an anti-matter particle was discovered for every fundamental particle of electric matter substance discovered in nature. This matter/anti-matter pair production reaction is always written in the form

$$\Delta E_{ph} = h\nu = mc^2 = E_x^M + E_x^{AM} \qquad (8)$$

where x is the fundamental particle with mass, h is Planck's constant, ν is the photon frequency and the subscript ph refers to photon.

Dirac received a Nobel prize for this work but scientists couldn't understand what "negative energy" means and thus chose not to follow his line of thought into the future.

Two concepts are useful to consider re the actual meaning of **negative energy**: (1) The first can be appreciated by consideration of Figure 5, which is a quantum mechanical calculation for the ten energy states associated with the formation of a Beryllium Dimer, Be_2, as two Beryllium atoms are brought close together.

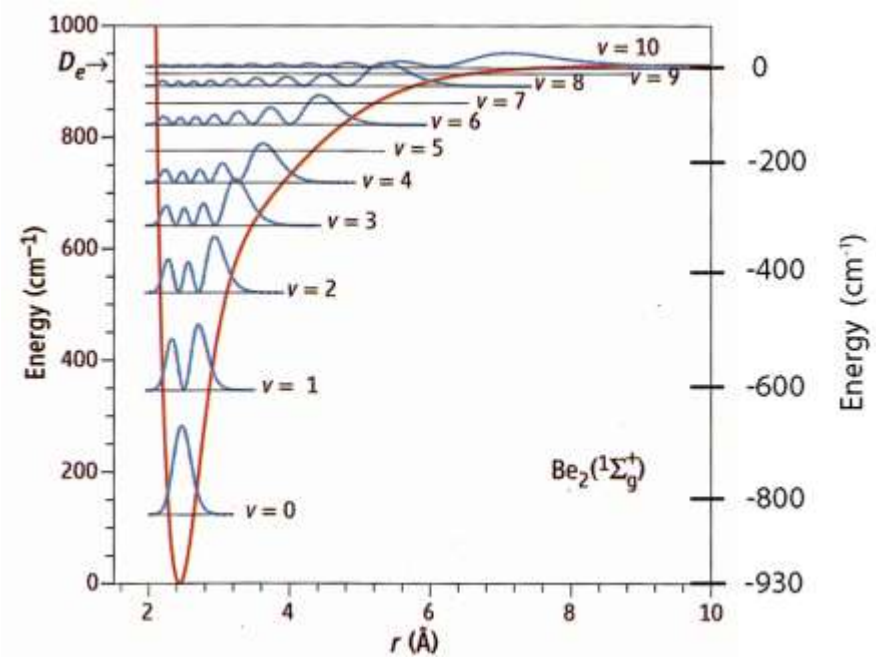

Figure 5. QM calculated energy states in the potential-well formed by the Be-Be Dimer reaction depending on the chosen origin of (1) r ≈ 2.4 A° or (2) r ≈ 9 A°.

Here, the usual origin for such a calculation is taken as the minimum position in the potential well so these quantum states are all positive **relative to** that origin. However, if we chose to take our origin at the Dimer dissociation position at $r \sim 9\dot{A}$, then all these quantum states would have negative energies relative to that new origin. Expanding on this concept, we might consider the possibility that what we call **God** has shaped a huge potential well (non-spatial or temporal) that holds the coarse physical vacuum somewhat like that illustrated in Figure 6.

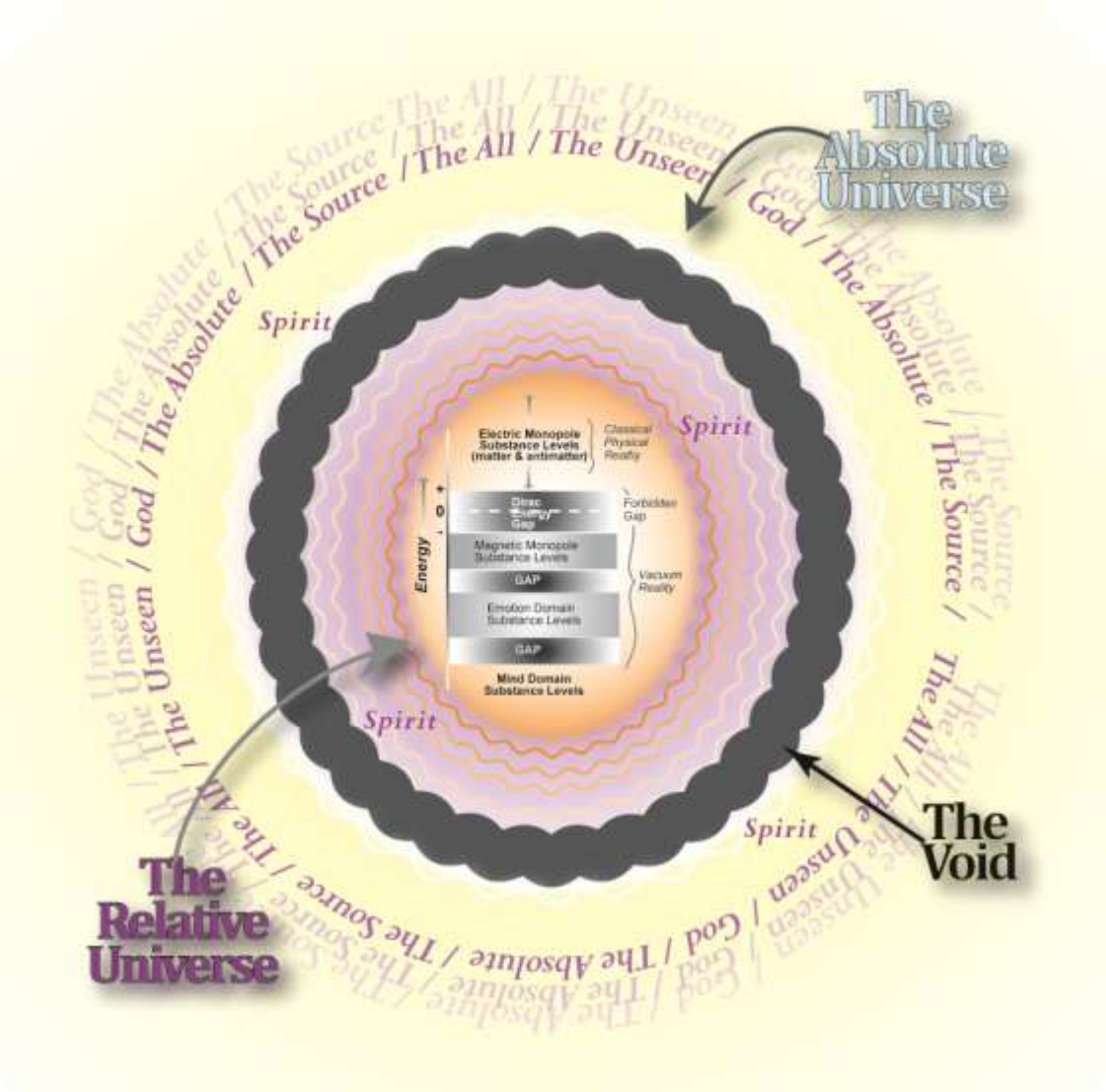

Figure 6. An energy level diagram embracing both the relative universe with expansion into the absolute universe lovingly guided by “the all”.

(2) An alternative possibility is to consider that the vacuum quantum states are all wave states which must be treated as waves and, as such, their energy must be considered as vectors of the mathematical form

$$E = R(k)e^{i\theta(k)} . \qquad (9)$$

Here, R is the wave amplitude, θ is the phase angle and k is the coordinate value. The amplitude is always positive and, if $o < \theta < \pi$, the second term in Equation 9 is also positive but, if $\pi < \theta < 2\pi$, the second term is negative so E is negative.

Let us now go back to topics (i), (ii) and (iii) and first consider the gravitational effects for $E^2>o$. The gravitational force, F_g, which is proportional to the product of the interacting masses, m_1 and m_2 i.e.,

$$F_g \propto \frac{m_1 m_2}{r} \qquad (10)$$

where r is their separation distance.

Case #1 (normal matter), E > o: $m_1 > o$, $m_2 > o$, v < c → **normal** gravitation for E > o
EM photons → **normal** gravitation for E > o

Case #2 (dark matter), E < o: $m_1 < o$, $m_2 < o$, v > c → **attractor** gravitation for E < o
ME photons → **attractor** gravitation for E < o

Case #3, $m_1 > o$, v < c, $m_2 < o$, v > c → repulsive force between massive amounts of dark matter in the cosmos center and a small amount of normal matter at the periphery of the expanding cosmos edge. This leads to acceleration rather than deceleration of the edge planets and stars.

For case #2, v > c is presumed, otherwise our astronomical instruments would have directly detected the "dark" matter rather than via only its gravitational presence.

To explain why, for any type of fundamental particle, the ratio of its matter/antimatter counterparts is greater than unity, one must first expand Figure 4 to include the substructure of Figure 7 for the physical vacuum.

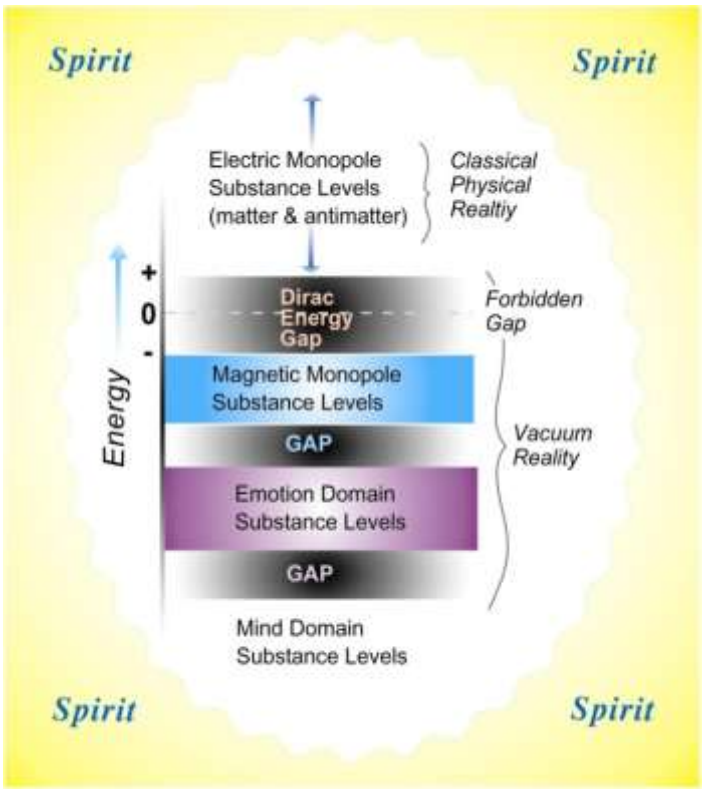

Figure 7. An energy level diagram embracing both classical physical substances and "unseen" vacuum substances.

These uniquely different energy bands of vacuum substance, magnetic information wave, emotion domain and mind domain, all imbedded in the domain of spirit, are thought to all be **prephysical** domains of substance of the invisible v > c category, i.e., existing before what has been labeled "the Big Bang". As such, both photons and other types of particles can be ejected upwards in the potential-well of the physical vacuum and fill some of these antimatter sites (hole sites) originally created via the Dirac-proposed process. This type of process would definitely annihilate some of these antimatter states changing them into uniquely new distinguishable states. Such a recombination type of process would yield matter/antimatter ratios greater than unity.

Postulates for Resolving the Dilemma

A new RF for viewing these coupled state, intention-induced phenomena of nature is seriously needed by today's science. In addition, because of the new experimental data, there must exist in nature a coupling agent that allows the v_w-waves to meaningfully interact with the v_g-wave group and the v_g-wave group with the v_p-particle. I have chosen to resolve all of these dilemmas via the proposing of four postulates:

1. The new RF for viewing physical reality is a duplex space consisting of two, four dimensional, **reciprocal** subspaces, one of which is space-time. Space-time is labeled D-space while its reciprocal subspace is labeled R-space.

2. This duplex physical RF is imbedded in an overall reality RF consisting of the three, higher dimensional domains of emotion, mind and spirit.
3. There exists in the domain of emotion, a moiety called “deltron”, that can be consciously activated, to serve as a **coupler substance** between the $v_p < c$ electric atom/molecule substances, the v_g substance and the $v_w > c$ magnetic information wave substance (see Figure 8).

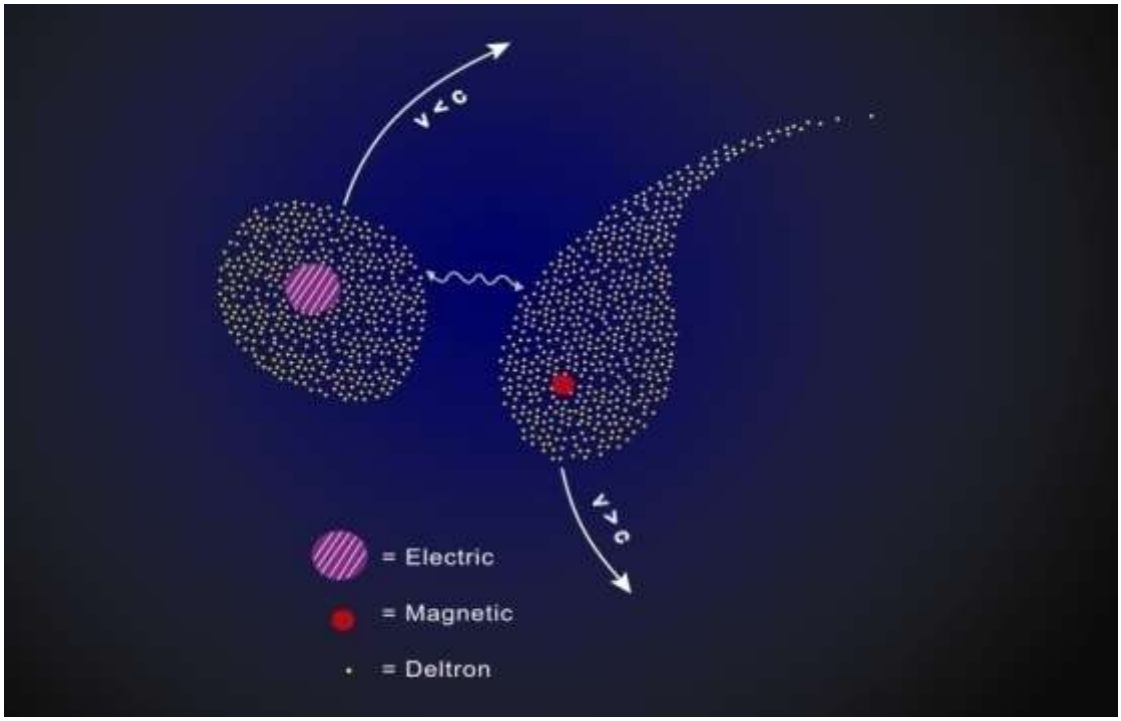

Figure 8. A higher dimensional level substance, labeled deltrons, falling outside the constraints of relativity theory and able to move at velocities $v \lessgtr c$, acts as a coupling agent between the electric monopole types of substances and the magnetic monopole types of substances to produce both electromagnetic (EM) and magnetoelectric (ME) types of mediator fields exhibiting a special type of “mirror principle” relationship between them.

4. The velocities of these three higher dimensional substances are also thought to be of the $v > c$ category so that interactive resonances can occur between them and R-space.

The relativistic view of conventional physical science concerning events happening in spacetime is to describe them using a Minkowski-space construct illustrated in Figure 9a.

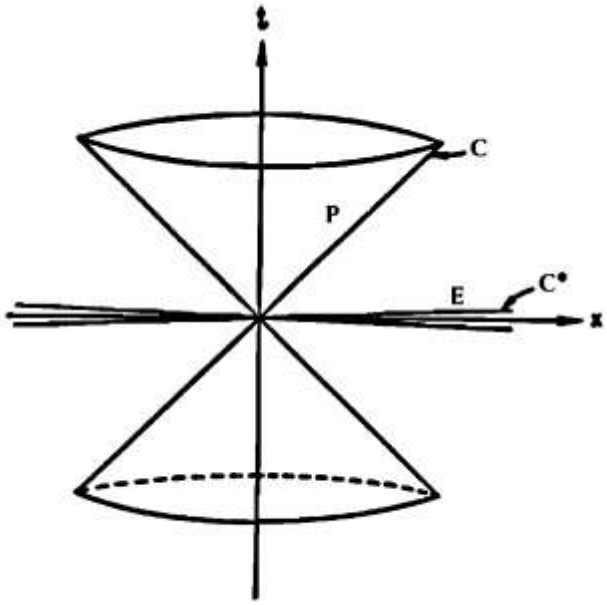

Figure 9a. Minkowski-type diagrams, (a) for the physical light come with v = c at the surface and the edge of the etheric light cone with $v = c^{*} >> c$ at its surface.

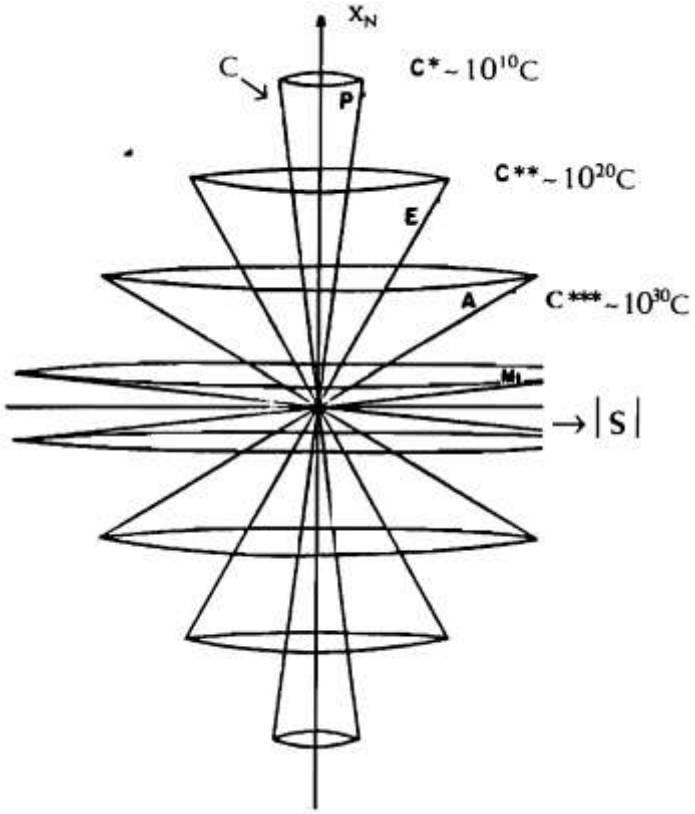

Figure 9b. A higher dimensional representation with X_N being the analogue of time, t, and $|S|$ being the analogue of distance, X, showing four light cone domains (P=physical, E=etheric, A=emotional and M_1=instinctive mind) with different surface signal velocities.

The origin is the “now”, the interior of the upper cones the future while that of the lower cone is the past. Any physical event occurring at v < c of the future takes place inside the upper cone (D-space) while events occurring at v = c take place on the walls of this cone (that is why it is labeled the “light cone”). The **exterior** of the inner cone labeled P_c out to the second cone, labeled P_F is R-space and together they form our new duplex-space RF. The subscripts C and F refer to coarse and fine, respectively. Figure 9b is an expansion of Figure 9a to include the next higher dimensions of emotion and mind. The assumption made here is the limiting velocity for each cone increases by a factor of about 10^{10} relative to the immediate light cone within it (higher dimensional “light”).

It is interesting to realize that the duplex space situation of Figure 9a plus Figure 4 yields an energy-velocity plot like that shown in Figure 9c.

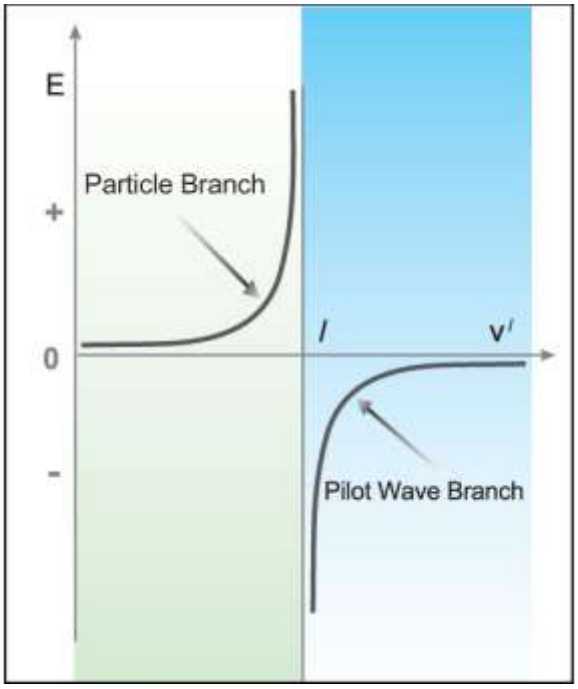

Figure 9c. Energy-velocity diagram for a D-space particle (v’ < 1 branch) and its R-space magnetic information wave conjugate (v’ > 1 branch).

This indicates that, if one tries to accelerate a positive mass particle to v = c, it will never attain such a state because it will tunnel through the potential barrier into the R-space negative energy state region. Thus, Einstein’s constraint is no longer a limitation. Likewise such tunneling can occur when a negative mass pilot wave approaches v = c from above.

Returning to our new duplex-space RF, the singular advantage of choosing the two subspaces as reciprocals of each other with one subspace being distance-time is that they have a very important mathematical relationship wherein any unique material property behavior of a substance in one subspace has an equilibrium conjugate property behavior in the reciprocal subspace. The mathematical quantitative connection between these two is called the Fourier Transform pair relationships[5]. For

example, if one knows quantitatively the time-dependent behavior of a specific material property in D-space, one can, in principle, calculate its R-space conjugate behavior.

The coordinates found to be useful for defining events in D-space are three perpendicular distances (x,y,z) plus a fourth imaginary distance, x^4=ict. The corresponding coordinates for R-space are all frequencies (ν_x, ν_y, ν_z, ν_t) where ν_x=l/x, ν_y=m/y, ν_z=n/z and ν_t=q/ict and l, m, n, q are unknown integers. If we think a bit, we will realize that the inversion of a distance is number per unit distance or a **spatial** frequency. Likewise the inversion of time is number per unit time or a **temporal** frequency. In today's solid state physics community, such a three-dimensional subspace RF is called **wave number space** and denoted by the vector (k_x, k_y, k_z). Thus for our duplex RF, we shall use the designation [(x,y,z,ict) α_{eff} (k_x, k_y, k_z, k_t/ict)] with α_{eff} yet to be discussed more fully. We already know that it is involved in coupling the substances of the two conjugate subspaces D-space and R-space together to some degree. A three-dimensional, duplex, reciprocal space is illustrated in Figure 10 to emphasize the reciprocal nature of these two different coordinate systems. Please note – they point in opposite directions.

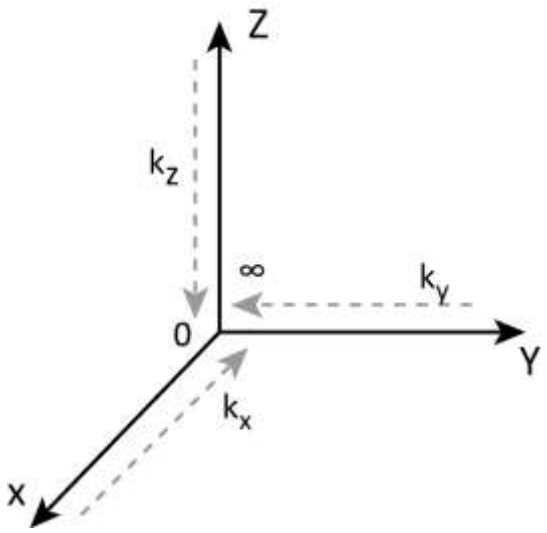

Figure 10. The duplex space coordinate systems (x,y,z) for D-space and (k_x, k_y, k_z) for R-space (note: they point n opposite directions).

The **Fourier Transform pair** relationships, and more importantly, the **deltron modulated Fourier Transform pair relationships** are so important that we understand, a good bit of space will be consumed in carefully describing its essential features.

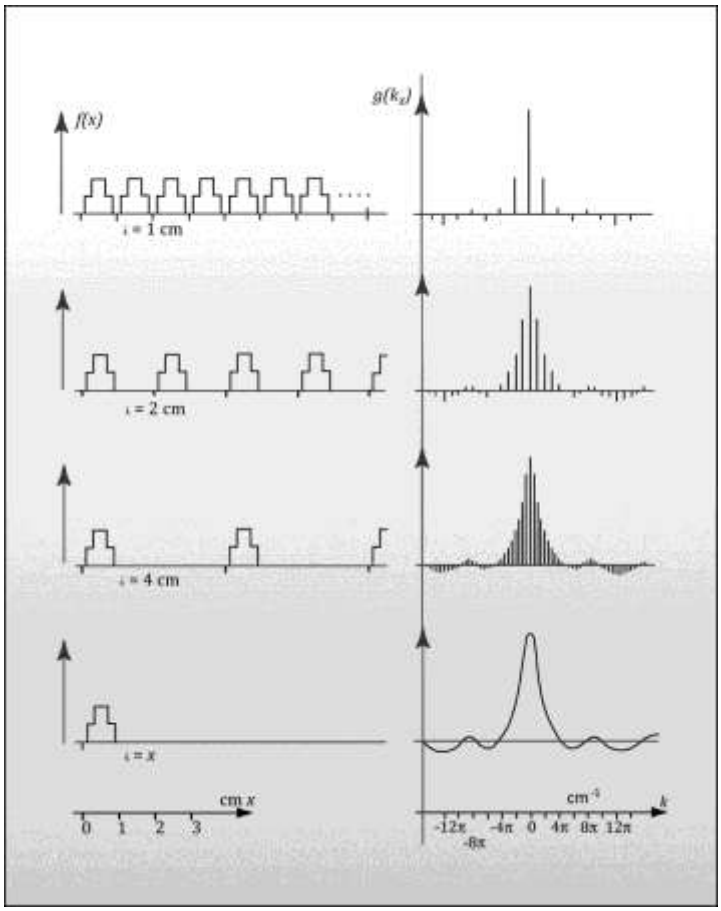

Figure 11. Illustrating the progression from Fourier Series to Fourier Transform.

The picture given in Figure 11 is the vehicle that we shall use to show how an R-space FT is developed from a D-space geometrical object. In D-space (left side), f(x) represents the mathematical form that quantitatively describes the periodic D-space object as a function of the D-space coordinate, x. In R-space (right side), the function, $g(k_x)$, represents the amplitude spectrum for the set of waves that describe the equilibrium conjugate for this object as a function of f(x). Here, each line is the amplitude of a simple harmonic wave (sine or cosine) at the specific frequency. As the D-space periodic length, λ, increases from $\lambda = 1$ centimeter (cm) to $\lambda = \infty$ cm, the R-space pattern fills in with vertical lines until only the envelope (ends of the lines) can be discerned. This plot of $g(k_x)$ at the bottom right is the **Fourier Transform** (wave amplitude distribution) of the bottom left object shape. It means that this specific D-space shape can be equally well described by this $g(k_x)$ shape in R-space. For the deltron-modulated Fourier Transform, the relationship is a little more mathematically complicated. All the rest is internally self-consistent mathematics.

To expand the reader's perspective on the equilibrium R-space intensity pattern associated with D-space objects, let us compare six simple two-dimensional D-space objects and their calculated R-space intensity patterns (the square of the calculated wave amplitude pattern for the corresponding Fourier Transforms). This comparison is presented in Figure 12.

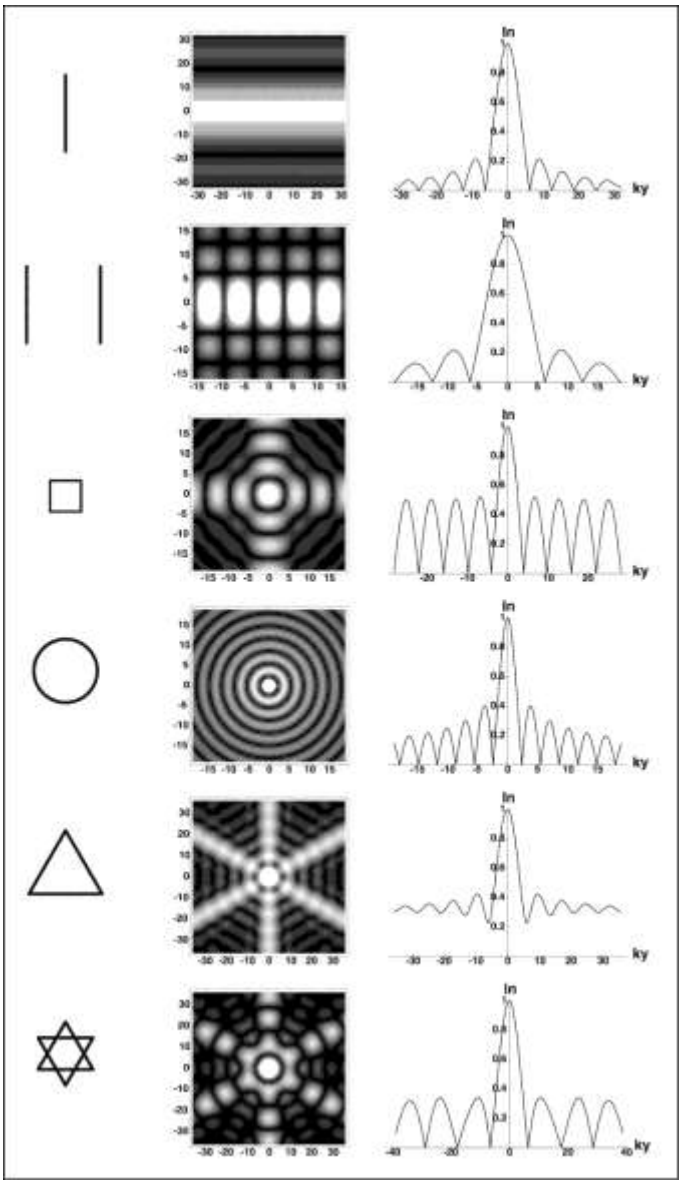

Figure 12. Comparison plots of R-space normalized modulus, l_n, for six, one-D objects (left column) versus (k_x, k_y) maps in the middle column versus a k_y or k_n section plot in the right column.

In the left column, the six objects represented are thin rod figures or thin slit figures cut in a solid background mask. In order from the top, they are a single rod, a pair of parallel rods, a square, a circle, an equilateral triangle and an interpenetrating, inverted pair of equilateral triangles. Mathematically, they represent a unique quality of substance having a pattern of contrast in the (x, y) plane. The Fourier Transform-calculated, corresponding two-dimensional, intensity patterns are shown in the central column of Figure 12 as (k_x, k_y) maps. The right hand column shows a vertical cut through the center of this (k_x, k_y) map to yield a normalized intensity, I_n, versus k_y map of the results.

The first thing one notices about the right hand column is that all the (I_n, k_y) plots are somewhat similar with a large magnitude central peak for I_n which quickly drops, in all cases but one, to zero amplitude at some small value of k_y and thereafter oscillates with decaying amplitude as one proceeds to larger k_y. The next thing one notices is that the shape profile of these secondary peaks are **quantitatively** different for each D-space object. In fact, if the size (length of side or radius) of the object becomes larger, the values of $k_y = k^*_y$, where $I_n = 0$, become smaller. Once again, one sees the reciprocal relationship appearing in the quantitative calculations.

The next important detail to notice is revealed by considering the central column and first comparing the top pattern with the second one down. When we do this we note that, the addition of a second parallel rod or slit at some spacing, λ, introduces an oscillatory pattern for I_n in the k_x-direction of some periodicity, Δk_x. Further, calculations show that, as λ increases in D-space, Δk_x decreases in R-space. Again, we see a reciprocal type of behavior occurring in these two, mathematical subspaces. This is to be expected from the wavelike-aspect of the substance that makes up the object and is called wave interference, constructive and destructive. Comparing the first and second columns of Figure 12, the reader can see that, every time there exists two parallel segments in the D-space object figure, wave interference develops in the R-space intensity pattern for the k-direction perpendicular to such segments.

Using this particular duplex-space perspective, one can see an entirely different explanation for the very famous Young's double slit experiment from the era of the classical mechanics paradigm. The conventional, single-space explanation (the old space and time explanation) saw the result as an interference of the light waves entering the two parallel slits and providing constructive/destructive superposition of these waves behind the slits. In that model, the slit structure itself contributes **nothing** but the two, parallel gap openings. This duplex-space perspective says that the slit structure itself, without the light waves, already has an R-space substance interference pattern existing around the slit regions of the D-space structure. The present hypothesis is that it is this R-space pattern that **guides** the light into its maxima and minima D-space intensity locations behind the slits.

This is one of those cases in science where two quite different models, each not fully understood in detail, provide satisfactory **qualitative** explanation for an experimentally observed phenomenon. Then, only by going to a comparison of the **quantitative** experimental details and the **quantitative** theoretical predictions of the two models can one decide which model is a better fit to the experimental data. Unfortunately, at this time, not enough is yet known concerning all the theoretical aspects of the duplex-space model proposed in this White Paper to be able to make a meaningful theoretical comparison. We will leave that for the future and, in the meanwhile, reserve judgment on this particular issue.

As an illustrative example of how one can optically generate Fourier Transforms for various two-dimensional object shapes consider Figure 13.

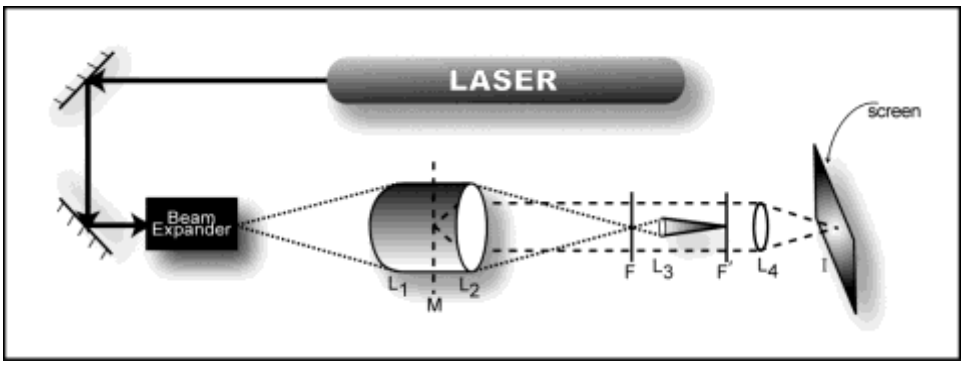

Figure 13. Experimental set-up used for generating the diffraction patterns at I from the mask, M (L_j = lenses and (F,F') = focal planes).

Here, one sees a laser beam that is expanded so as to pass through a pair of lenses (L_1, L_2), in the middle of which is a metal mask, M, that has a particular pattern drilled through it. The coherent light passes through and is diffracted from the particular pattern shape before being focused onto the screen. The intensity (the amplitude squared) of the light impinging on F is the diffraction pattern of the light by the object of the mask (also like the Fourier Transform of this object mask[6]). Let us look at some of these so as to learn something about the D-space object shape and Fourier Transform pattern relationships. A comparison between hole geometry in a mask, M, and the diffraction pattern on the screen from Harburn et al's study[6] is provided in Figure 14 for a few cases. What is recorded at F' of Figure 13 is the intensity of the diffraction pattern and this is the amplitude squared of the Fourier Transform FT, not the Fourier Transform itself.

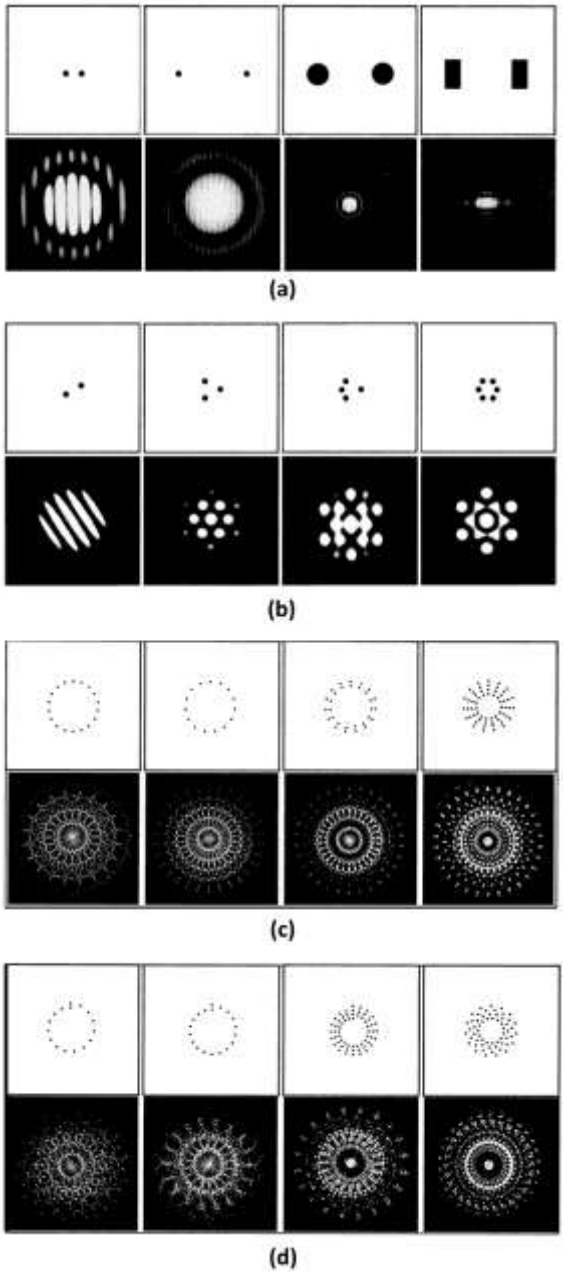

Figure 14. The mask with holes is our D-space object and the diffracted wave intensity pattern focused onto a screen is intimately connected to its R-space counterpart. As size goes up in one, it goes down in the other; as separation increases in one, it decreases in the other; as clockwise rotation occurs in one, equal counterclockwise rotation occurs in the other and shape changes in a particular direction for one leads to changes in the perpendicular direction for the other. The mandala-like diffraction intensity patterns are similar to what many individuals see internally in their mind's eye while in a deep state of meditation.

The top panel in Figure 14a shows masks with two holes of different size, shape and spacing. The lower panel in Figure 14a shows the diffraction pattern corresponding to each mask above. From these two rows, one can see how (1) increasing the D-space hole spacing, reduces the spacing (increases the frequency) of the perpendicularly oriented vertical fringes that are observed in the basic ring pattern from a single hole; (2) increasing the diameter of the D-space hole decreases the diameter of the segmented ring pattern; (3) rotating the orientation of the axis between the two holes in one direction, rotates the segmented ring pattern in the opposite direction by the same amount; (4) rectangular D-space holes in one direction lead to elliptical ring-shaped patterns in the perpendicular direction; and (5)

increasing the number and symmetry of the D-space holes increases significantly the complexity of the diffraction pattern.

The richness of detail in the R-space diffraction patterns that occur from a D-space set of holes in a circular or spiral pattern is illustrated in Figures 14c and 14d, respectively. These mandala-like patterns are similar to what many individuals see internally with their "mind's eye" while in a deep state of meditation. In this regard, it makes one wonder about D-space/R-space sensory perception.

In Figure 14b, the experimentally-generated diffraction pattern for a D-space hexagon of holes is given. To prove to the reader that the Fourier Transform truly represents the diffraction pattern, we calculate the normalized R-space intensity (square of the amplitude) spectrum for this D-space hexagon of holes so as to compare it with the experimentally-generated diffraction pattern. Figure 15 shows this comparison and completely supports the assertion that the Fourier Transform quantitatively reproduces the diffraction result for specific cases.

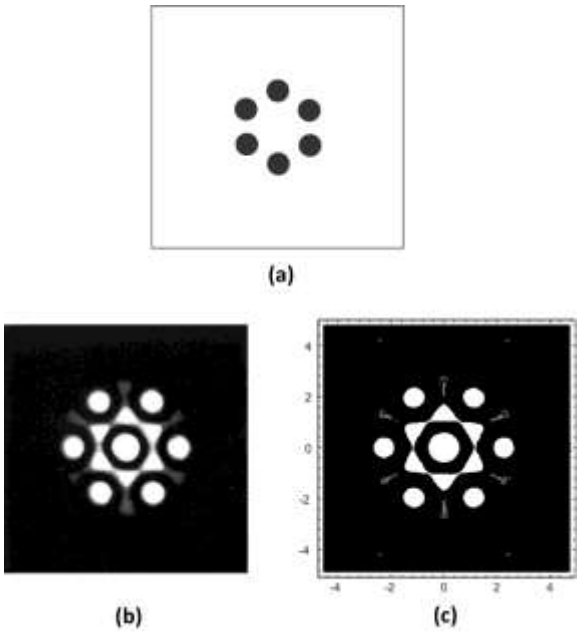

Figure 15. (a) The hexagonal arrangement of a circular hole mask used in Figure 14, (b) the experimentally observed diffraction pattern from (a), and (c) the I_n pattern calculated via the Fourier Transform of (a).

All of the foregoing is an expansion of detail connecting the D-space RF to the inverse nature of the R-space RF. Regions very far from us in D-space occupy the very low frequency region of R-space so that they are likely to be interactive with each other in R-space although not very likely in D-space. If we were to call our D-space sun the origin, just for example, and label it as (0, 0, 0, t), one could project outwards to the stars and further towards infinity. If, at the same time, we evaluate an R-space perspective, we find that a D-space infinity coincides with the zero wave number (frequency) region of R-space and this D-space origin corresponds with the R-space infinite frequency region. Thus, there appears to be a kind of infinite loop, wholeness to this particular duplex space.

Information Transformation in the Brain

Pribram[7] has written extensively on the brain processes involved in imaging and has a Holonomic theory to explain them. It is based solely on a slight modification of the Fourier Transform duality between D-space information patterns and spectral domain information patterns. An overly simplistic picture would be that a spacetime information pattern enters the body via the circular lens of the eye. Eventually, it activates the input and operator neurons of the brain's cortical columns. This leads to overlapping receptive fields of interneurons that are tunable by adaptation and habituation. Each interneuron thus acts like a bin in a computer that stores the averages of

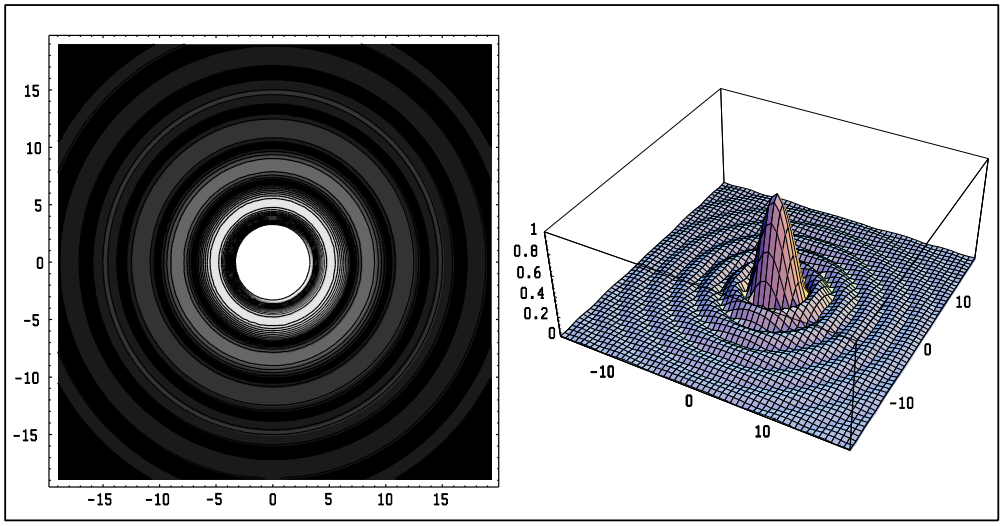

Figure 16. Topographic and section perspectives of normalized modulus, I_n.

the part of the patterns of input to which it is exposed[7]. The ensemble of receptive fields (bins) stores the average pattern and, when one plots these receptive fields, they bear a marked correlation to the Fourier Transform of the spacetime pattern impinging on the iris of the eye. For a uniform light intensity impinging on a circle (the iris of the eye), the Fourier Transform is given in both sectional and contour plots by Figure 16 and this pattern is a good representation of Pribram's experimental results[7].

The summary view, then, is that cortical neurons act like individual receiving antennas in a large array converting the spacetime information into a diffraction pattern whose mathematical representation is very close to the particular Fourier Transform. This information conversion to the frequency domain appears to be ideal for subsequent brain processing and brain perception. In the general area of antenna arrays, whether of the receiving or transmitting type, there exists the "principle of pattern multiplication" which may be stated most generally as follows: The total field pattern of an array of nonisotropic but similar sources (sinks) is the product of the individual source pattern and the pattern of an array of isotropic point sources (sinks) located at the phase center of the individual source and having the same relative amplitude and phase, while the total phase pattern is the sum of the phase patterns of the individual sources and the array of isotropic point sources. In electrical engineering, this general concept has been expanded to consider a continuous array of point sources (separated from

each other by infinitesimal distances) which has been found to be equivalent to a continuous field or "aperture" distribution for an antenna[8]. One finds that it is the Fourier Transform relationship that connects the far field radiation pattern and the aperture distribution just as we found via Figure 15 for the simple array of six holes in a mask.

The purpose of this last section on the Fourier Transform results, which are mathematically exact, is to allow the reader to obtain a meaningful perspective of what to expect to see from R-space patterns manifesting in our duplex-space RF as deltron coupling grows within us in the near future. Without **any** deltron coupling, we cannot evolve to R-space awareness because the v<c substances cannot meaningfully interact with the v>c substances in nature and we are locked into a distance-time only awareness of nature. As the deltron population grows within us, **so also** does deltron coupling between D-space substances and R-space substances so that more and more will we perceive well-developed R-space patterns. For example, the digital camera manifestations of the "orbs" phenomena() seen my many, many people around the world is just such an indicator that heralds a necessary orthodox science shift to this type of duplex space RF shift.

The mathematical shift from historical Fourier Transforms to deltron-modulated Fourier Transforms is a necessary step in our human tools development to enrich our understanding of R-space. This will unfold via a series of steps wherein a series of mathematical approximations will be made for $\alpha_{eff}(t)$ in Equation (1). The first step will be with $\alpha_{eff}(t) \approx$ a constant so that the historical Fourier Transform is used to generate an approximate R-space pattern but with an average magnitude shift via a constant α_{eff}.

In one-dimension, the historical Fourier Transform pair relationships are given by the mathematical expressions (see Figure 11),

$$g(k_x) = \left(\frac{1}{2\pi}\right)^{1/2} \int_{-\infty}^{+\infty} f(x) e^{+ix\cdot k_x}\, dx \qquad (11a)$$

$$f(x) = \left(\frac{1}{2\pi}\right)^{1/2} \int_{-\infty}^{+\infty} g(k_x) e^{-ix\cdot k_x}\, dk_x \qquad . \qquad (11b)$$

Here, f(x) is the D-space pattern, while $g(k_x)$ is its conjugate R-space pattern. Its R-space intensity, $I(k_x)$ at the R-space coordinate, k_x, is the more physically meaningful pattern to perceive and is given by

$$I(k_x) = [g(k_x) g^*(k_x)]^{1/2} \qquad (11c)$$

where g^* is called the complex conjugate of g. This means that every time the imaginary number, $+i$, appears in g, it is to be replaced by, $-i$. This allows I at any location of R-space, k_x, to be a positive number (like R in Equation 9).

Expanding the picture to the next step of the deltron-modulated Fourier Transform we first need to choose a trial deltron coupling function, $\delta_c(x,k_x)$, which is a mathematical unknown to us, to ultimately be determined by later matches between theory and experiment. For simplicity, let us initially choose, δ_c as

$$\delta_c\left(x,k_x\right)=\sum_n a_n^{\delta}e^{inw^{\delta}x}\ , \tag{12a}$$

and our first step in the approximations to be taken will be

$$\delta_c(x,k_x)\approx a_o^{\delta}\approx\alpha_{eff}=constant \tag{12b}$$

so that the zeroth-approximation to the deltron-modulated Fourier Transform will be given by

$$g_o(k_x)\approx\frac{a_o^{\delta}}{(2\pi)^{1/2}}\int_{-\infty}^{\infty}f(x)e^{+ix\cdot k_x}\,dx \tag{12c}$$

$$f(x)\alpha_{eff}=\frac{1}{(2\pi)^{1/2}}\int_{-\infty}^{\infty}g_o(k_x)e^{-ix\cdot k_x}\,dk_x\quad . \tag{12d}$$

This would be naturally followed by the first-order approximation to the deltron-modulated Fourier Transformation,

$$g_1(k_x)\approx\frac{1}{(2\pi)^{1/2}}\int_{-\infty}^{+\infty}f(x)\left(a_o^{\delta}+a_1^{\delta}e^{-iw^{\delta}x}\right)e^{+ix\cdot k_x}\,dx \tag{12e}$$

$$f(x)\left(a_o^{\delta}+a_1^{\delta}e^{iw^{\delta}x}\right)\ \approx\frac{1}{(2\pi)^{1/2}}\int_{-\infty}^{+\infty}g_1(k_x)e^{-ix\cdot k_x}\,dk_x. \tag{12f}$$

Ultimately, we would reach the complete mathematical description of the deltron-modulated Fourier Transform (for this particular trial function for $\delta_c(x,k_x)$) as

$$g_n(k_x)\approx\frac{1}{(2\pi)^{1/2}}\int_{-\infty}^{+\infty}f(x)\sum_{n=o}\left(a_n^{\delta}\ e^{inw^{\delta}x}\right)e^{+ix\cdot k_x}dx\ , \tag{13a}$$

$$f(x)\sum_{n=o}a_o^{\delta}\ e^{+inw^{\delta}x}=\frac{1}{(2\pi)^{1/2}}\int_{-\infty}^{+\infty}g_n(k_x)e^{-ix\cdot k_x}\,dk \tag{13b}$$

As one follows this mathematical procedure, one will learn more and more about **one aspect** of R-space and our unfoldment process plus its relationship to the second and third rungs of our "ladder of understanding" (see Figure 1). Just as our development of pH-measurements of water as an investigative tool for the study of higher dimensions in physical reality, the theoretical study of the historical Fourier Transform mathematical technique has led us to an investigative tool for the study of R-space nature and our inner unfoldment as a developing species.

As stated many times, in our proposed duplex space, the deltron coupling substance **must be present** to allow a substance quality of one subspace to actually **interact** with the conjugate substance quality of the reciprocal subspace.

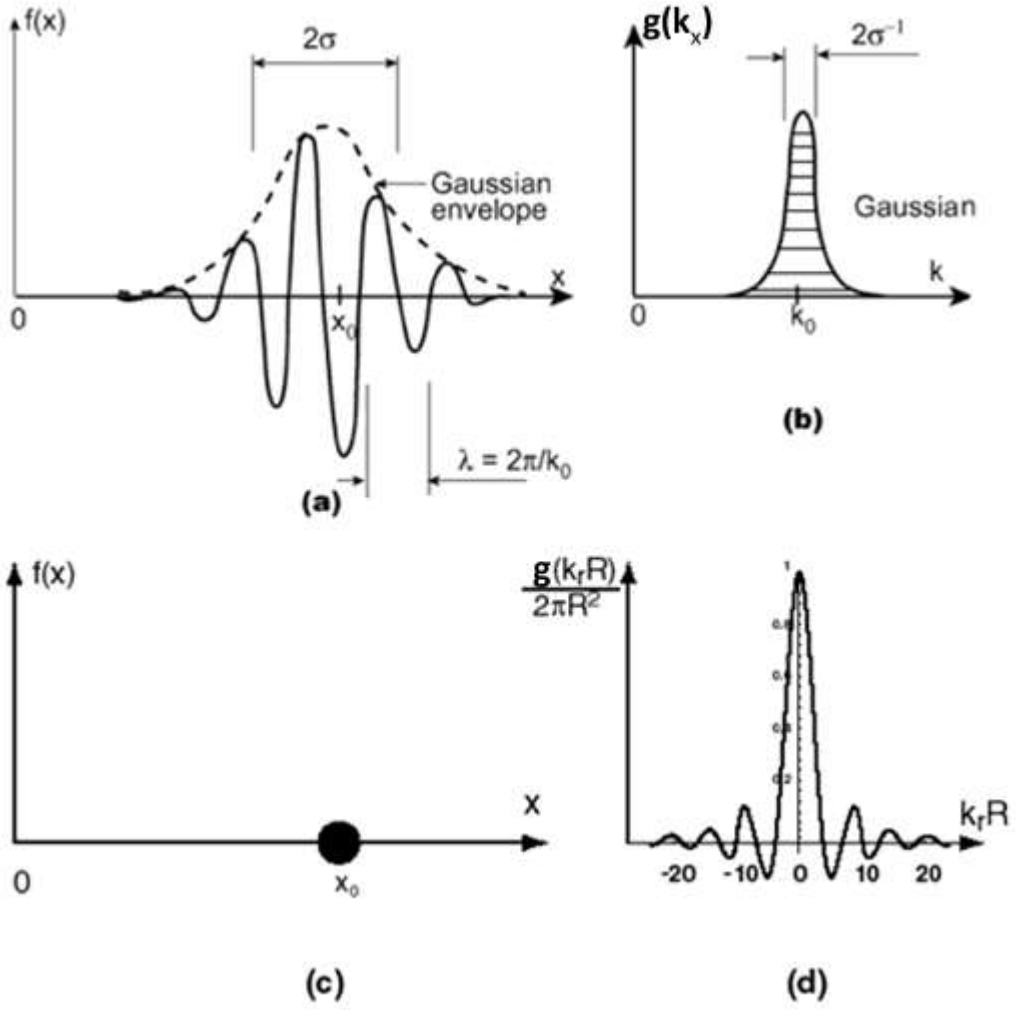

Figure 17. (a) a "ghost" calculated D-space wavegroup for (b) a real R-space, Gaussian substance packet, (c) a real D-space 2-D particle of radius R and (d) its "ghost" calculated R-space conjugate wavegroup. For an atom, one would choose $R \sim 10^{-8}$ cm.

Without the deltron coupling, the thermodynamic equilibrium between the two uniquely different kinds of substance can never be achieved. For example, in Figure 17, the top portion in (b) a Gaussian-shaped packet or reciprocal space substance, $g(k_x)$, (Equation 13a), generates in (a) an FT-wave group also of Gaussian-envelope shape in D-space, (f(x) in Equation 13b). The bottom portion of Figure 17 shows in (c) a spherical particle of D-space substance, (a different f(x) in Equation 13a), while (d) shows its $g(k_x)R/2\pi R^2$ R-space counterpart. Here R is the D-space particle radius. Here items (b) and (c) are actual substances in their respective domains while items (a) and (d) are calculated **ghost patterns** unless

sufficient deltrons are added so that the substances can interact with each other and we have a functional DeBroglie particle/pilot wave system in both subspaces that can seek thermodynamic equilibrium between its distinguishable parts.

Before leaving this FT-topic, let me leave just a hint of its profound utility in the future investigation of today's anomalous human cognition labeled "remote viewing". Paul Werbos, a PhD student of Nobelist Julian Schwinger and director of engineering for NSF in the U.S. made a very prophetic statement about a decade ago[9]. He stated that:

(1) All forms of quantum electrodynamics –Copenhagen, Bohmian, Schwinger-type or Werbos-type yield the same kind of predictions and **none** of them can explain something like "remote viewing". This author believes that this statement applies to **any psychoenergetic phenomenon!**

(2) Werbos also tells us that the world has spent billions of dollars to use quantum electrodynamics in the military to see things very far away and it has completely failed to do so. The present author takes this to mean that our present day formulation of quantum mechanics, great as it is for D-space phenomena, is totally inadequate to encompass the inclusion of psychoenergetic phenomena into our scientific world view. The latter requires an expansion of our RF, as a first step, to the presently proposed duplex-space RF because all psychoenergetically-based natural phenomena appear to be R-space and higher-dimensionally dependent. In this same category, (1) the human unconsciousness, (2) the human acupuncture/meridian system, (3) the human chakra system and (4) homeopathy are expected to be found.

Metastable vs. Stable Thermodynamic Equilibria

Using a variety of force fields and dynamic technologies, we can create thermodynamically metastable state materials as distinct from thermodynamically equilibrium state materials (diamonds, lasers, multilayer solids, coupled duplex space materials, etc). Their stable lifetime requires the maintenance of some unusual thermodynamic force to be present in the local environment for that lifetime. For a laser, the continuous pumping of light of appropriate frequency and intensity is required. For a coupled duplex space, periodic re-imprinting of the intention host device (IHD) is required to maintain a sufficient dynamic population of deltrons in the locale for coupling between $v < c$, $E > o$ materials and $v < c$, $E < o$ materials to readily occur. With our present IHD technology, deltrons leak away from the "conditioned" space and must be continuously replenished for the anomalous material property behavior to stay stable. One of the important thermodynamic factors involved is called the **gauge symmetry state** of the space. The importance of this factor and even knowing what it technically means is very poorly appreciated by the general human community so that is one topic that we need to address here (there are others).

The Gauge Symmetry Concept

The concept of gauge was introduced in 1918 by Herman Weyl to mean a standard of length whereby the gravitational force could be formulated in terms of the curvature of space and the various

geometries involved. In general, Gauge Theories were constructed to relate the properties of the four known fundamental forces of nature to the various symmetries of nature (see Figure 18[10]). The most familiar symmetries are spatial or geometric in appearance, like the hexagonal symmetry of a snowflake. An invariance in the snowflake pattern occurs when it is rotated by 60 degrees. In general, the state of symmetry can be defined as an **invariance** in pattern that is observed when **some** transformation is applied to it (e.g., a 60° rotation for the snowflake or a 90° rotation for a square).

One example of a non-geometric symmetry is the charge symmetry of electromagnetism. For the case of a collection of electric dipoles, if the individual charges are suddenly reversed in sign, the energy of the ensemble is unchanged so the forces remain unchanged. The same behavior occurs for magnetic dipoles and electromagnetic fields in general (this is because the energy is proportional to E^2 and to H^2 so it does not change by a 180° rotation of the dipoles). Another symmetry of the non-geometric kind relates to isotopic-spin of particles, a property of neutrons, protons and hadrons (the only particles responsive to the strong nuclear force). The symmetry transformation associated with isotopic-spin rotates the internal indicators of all protons and neutrons everywhere in the universe by the same amount and at the same time. If the rotation is by exactly 90 degrees, every proton becomes a neutron and every neutron becomes a proton so that no effects of this transformation can be detected and this symmetry is invariant with respect to isotopic-spin transformation.

All of these described symmetries are global symmetries (happening everywhere at once). In addition to global symmetries, which are almost always present in a physical theory, it is possible to have a local symmetry[11]. For a local symmetry to be observed, some law of physics must retain its validity (remain invariant) even when a different transformation takes place at each separate point in space-time. Gauge Theories can be constructed with either a global symmetry or a local symmetry (or both). However, in order to make a theory invariant with respect to a local transformation something new must be added. This new something is a new force[11].

The first Gauge Theory with local symmetry was the theory of electric and magnetic fields, introduced in 1868 by James Clerk Maxwell. The character of the symmetry that makes Maxwell's theory a Gauge Theory is that the electric field is invariant with respect to the addition or subtraction of an arbitrary overall electric potential. However, this symmetry is a global one because the result of experiment remains constant only if the new potential is changed everywhere at once (there is no

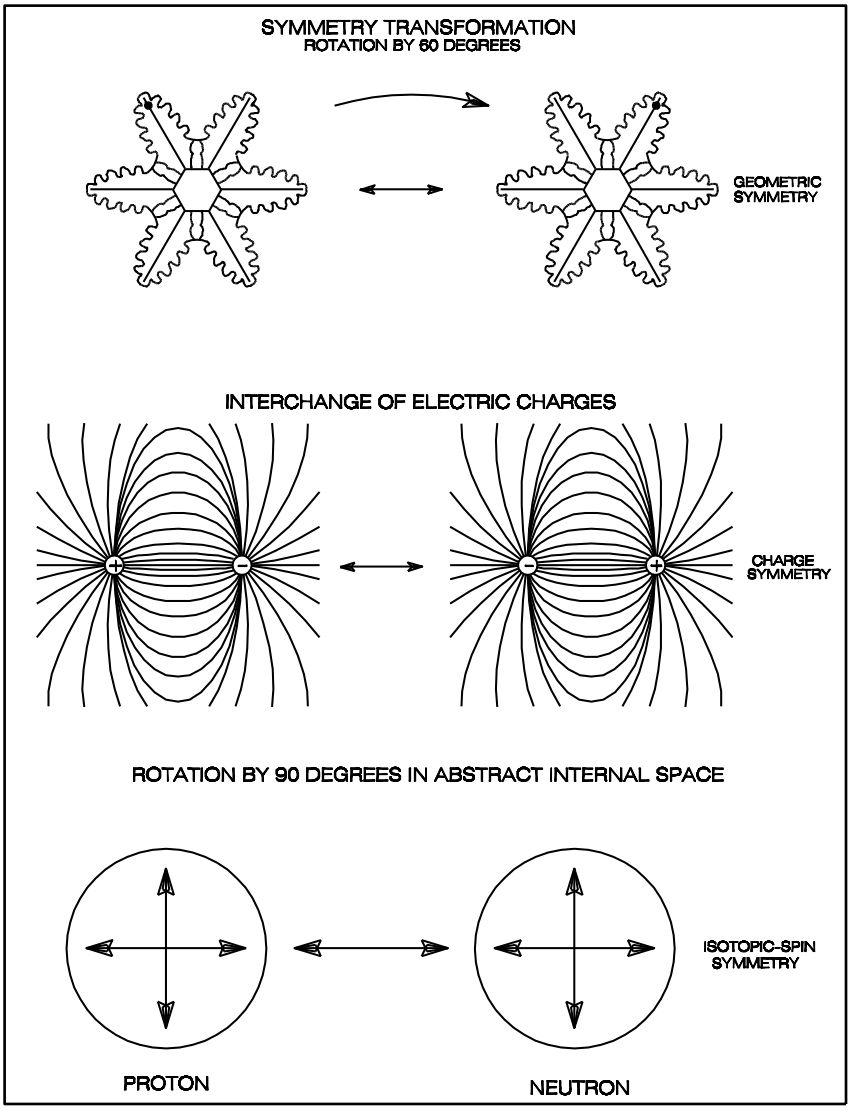

Figure 18. Symmetries of nature determine the properties of forces in Gauge theories. The symmetry of a snowflake can be characterized by noting that the pattern is unchanged when it is rotated 60 degrees; the snowflake is said to be invariant with respect to such rotations. In physics, non-geometric symmetries are introduced. Charge symmetry, for example, is the invariance of the forces acting among a set of charged particles when the polarities of all the charges are reversed. Isotopic-spin symmetry is based on the observation that little would be changed in the strong interactions of matter if the identities of all protons and neutrons were interchanged. Hence proton and neutron become merely the alternative states of a single particle, the nucleon, and transitions between the states can be made (or imagined) by adjusting the orientation of an indicator in an internal space. It is symmetries of this kind, where the transformation is an internal rotation or a phase shift, which are referred to as Gauge symmetries.

absolute potential and no zero reference point). A complete theory of electromagnetism requires that the global symmetry of the theory be converted into a local symmetry. Just as the electric field depends ultimately on the distribution of charges, but can conveniently be derived from an electrical potential, so the magnetic field generated by the motion of these charges can be conveniently described as resulting

from a magnetic potential. It is in this system of potential fields that local transformations can be carried out leaving all the original electric and magnetic fields unaltered. This system of dual, interconnected fields has an exact local symmetry even though the electric field alone does not[(11)].

Maxwell's theory of electromagnetism is a classical one, but a related symmetry can be demonstrated in the quantum theory of EM interaction (called quantum field theory). In the quantum theory of electrons, a change in the electric potential entails a change in the **phase** of the electron wave and the phase measures the displacement of the wave from some arbitrary reference point (the difference is sufficient to yield an electron diffraction effect). Only differences in the phase of the electron field at two points or at two moments can be measured, but not the absolute phase. Thus, the phase of an electron wave is said to be inaccessible to measurement (requires a knowledge of both the real **and** the imaginary parts of the amplitude) so that the phase cannot have an influence on the outcome of any possible experiment. This means that the electron field exhibits a symmetry with respect to arbitrary changes of phase. Any phase angle can be added to or subtracted from the electron field and the results of all experiments will remain invariant. This is the essential ingredient found in the U(1) Gauge condition.

Although the absolute value of the phase is irrelevant to the outcome of experiment, in constructing a theory of electrons, it is still necessary to specify the phase. The choice of a particular value is called a Gauge convention. The symmetry of such an electron matter field is a global symmetry and the phase of the field must be shifted in the same way everywhere at once. It can be easily demonstrated that a theory of electron fields, along with no other forms of matter or radiation, is **not** invariant with respect to a corresponding local Gauge transformation. If one wanted to make the theory consistent with a local Gauge symmetry, one would need to add another field that would exactly compensate for the changes in electron phase. Mathematically, it turns out that the required field is one having infinite range corresponding to a field quantum with a spin of one unit. The need for infinite range implies that the field quantum be massless. These are just the properties of the EM field, whose quantum is the photon. When an electron absorbs or emits a photon, the phase of the electron field is shifted[(12,13)].

The gauge symmetry case of our interest in this white paper is the one where we have two unique levels of physical reality as indicated in Equation 1. In one, we have electric atoms and molecules restricted to travel at velocities less than that of c, the velocity of EM light. In the other, we have magnetic information waves restricted to travel at velocities greater than c. Our main interest, here, is how one describes the EM gauge symmetry state for the two cases (1) these two levels of physical reality are almost completely uncoupled and (2) these two levels are strongly coupled so that the second level is instrumentally accessible via the measuring instruments of the first.

In the first case, one could define a generalized potential function, Ψ, and EM gauge symmetry state where

$$\Psi = \Psi_D (x, y, z, t) + \Psi_R (k_x, k_y, k_z, k_t) \quad (14a)$$

and EM gauge state: $U_e(1) + U_m(1)$ (14b)

However, our commercial measurement devices, cannot access the phenomena associated with Ψ_R so it doesn't exist to us.

In the second case, a strong coupling coefficient, α_{eff}, exists between e and m substances so we have

$$\Psi = \Psi(x, y, z, t, \alpha_{eff}, k_x, k_y, k_z, k_t) \quad (15a)$$

And, perhaps

$$\text{EM gauge state: } U_e(1) \times \alpha_{eff} \times U_m(1) = SU(2) \quad (15b)$$

Now let us see how to interpret these EM gauge states.

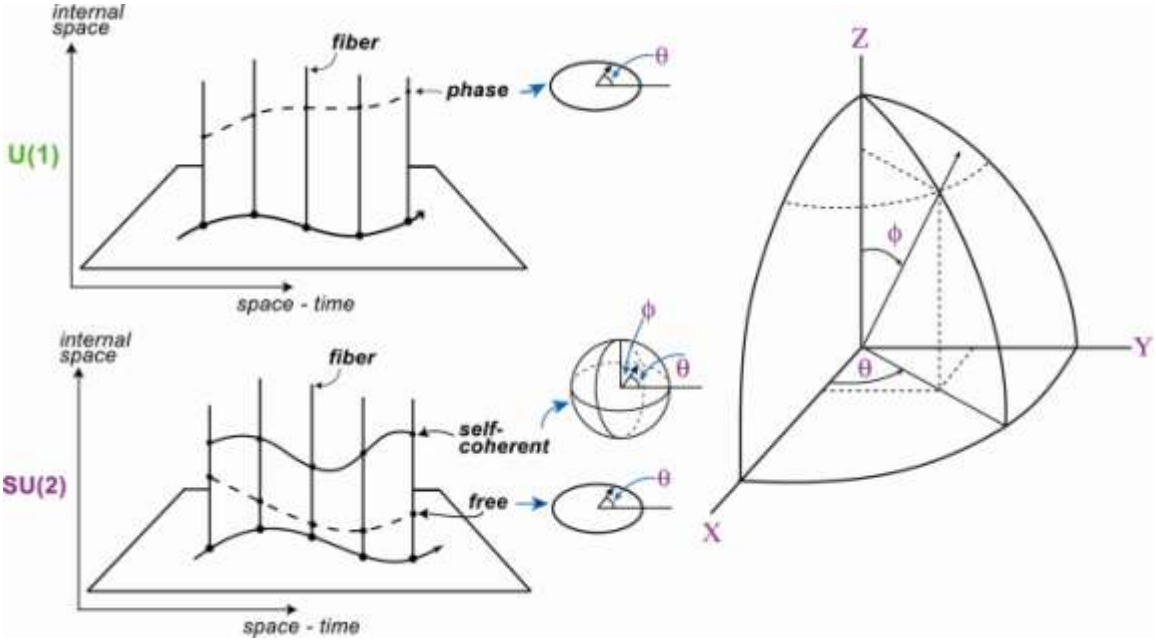

Figure 19. Illustrations crucial to meaning articulation for the U(1) and SU(2) EM gauge symmetry states.

Consider the top drawing in Figure 19, it shows a unique space that combines an internal space (ordinate) with a two-dimensional representation of spacetime (abscissa). In this unique space, the spatial location of a particle is represented by a dot at a coordinate point in the horizontal, spacetime plane while the phase-value for the field in the internal space is specified by angular coordinates in this unique space. As the particle moves through spacetime (the sequence of dots), it also traces out a path in the internal space (the dashed line) above the spacetime trajectory at a distance proportional to the instantaneous phase angle for the electron wave. Mathematicians call this internal space distance a fiber.

When there is no external gauge potential acting on the particle, the internal space path is completely arbitrary. When this particle interacts with an internal gauge field (E or H), the dashed path

in the internal space is a continuous curve determined by the gauge potential. In mathematical jargon, the unique space formed by the union of our four-dimensional spacetime with an internal space is called a "fiber bundle space" [(12)]. When there is only one internal space variable, like the electron wave function, the internal space is designated as a U(1) EM gauge symmetry space because the state looks like the interior of a flat ring with the phase value represented as the angle, θ, of the point on the ring seen in Figure 19 (top).

When there are two coupled variables in the internal space, such as the electron particle wave function, θ, and the magnetic information wave, wave function, ϕ, they must each make perpendicular plane designations in a sphere at each spacetime point as seen in the bottom drawing of Figure 19. Thus, one has two fiber bundles to deal with and the group theory designation is SU(2). The lower internal space locus in the bottom diagram of Figure 19 is labeled free because it is a U(1) state with only one phase angle, θ, to deal with. The upper internal space locus is labeled coherent because it is a SU(2) state with two phase angles, θ and ϕ, to deal with. What is called symmetry breaking is when the coupling between θ and ϕ disappears so the symmetry state drops from the upper locus to the lower.

Both the U(1) and the SU(2) gauge state use group theory notation. U(1) is an example of the continuous group because each element of U(1) is characterized by a unique phase angle, θ, which is a continuous parameter, hence the name, continuous group. The SU(2) gauge is a member of the special unitary or unmodular group, SU(n). The elements of SU(n) have n^2-1 independent parameters. For example, the neutron $\leftrightarrow$ proton exchange reaction, which also requires neutrino involvement, is also a member of the SU(2) group with its isospin symmetries. Likewise, the SU(3) gauge state has 3^2-1 = 8 independent parameters which Nobelist Gell-Mann called "the 8-fold way" in quantum chromodynamics that deals with quark interactions.

As particle physicists progress into serious investigations of gauge symmetry states, they bump into the need to expand their quantitative assessments from vectors and Abelian algebra ($\underline{AB}$-$\underline{BA}$ = o) to quaternions and non-Abelian algebra ($\underline{AB}$-$\underline{BA}$ ≠ o). The reader of this White Paper may think that this is not important for them to understand because they are not really interested in fundamental particle physics, they are more interested in the human body with (1) normal skin, (2) skin with acupuncture points, (3) the acupuncture meridian system, (4) the human chakra system, (5) healing of these systems in humans, (6) etc.

This author does not mean to burden the reader with complex mathematics for its own sake. However, if one chooses to seriously study human science, these topics cannot be avoided. Although the human skin, cells, muscles and organs appear to all be U(1) gauge material; we were able to show that the acupuncture meridian system is at the SU(2) gauge level[(12)] and we expect the human chakra system to be at an even higher gauge level. Therefore, for serious study of such human body systems, non-Abelian algebra plus quaternion considerations will be needed.

A New Experimental Tool – Converting our pH-measurement Device to a Subtle Energy Detector

One of the very useful results of our experimental studies is that one can now quantitatively measure the **excess** thermodynamic free energy per unit volume, $\delta G^*_{H^+}$, of an IHD-conditioned space,

relative to the U(1) gauge symmetry state (normal thermodynamics) for the aqueous hydrogen ion, H^+. Therefore, all of our pH-measurements can be mathematically scaled to this standard. On the experimental side, we used a pH-probe system like that illustrated in Figure 20.

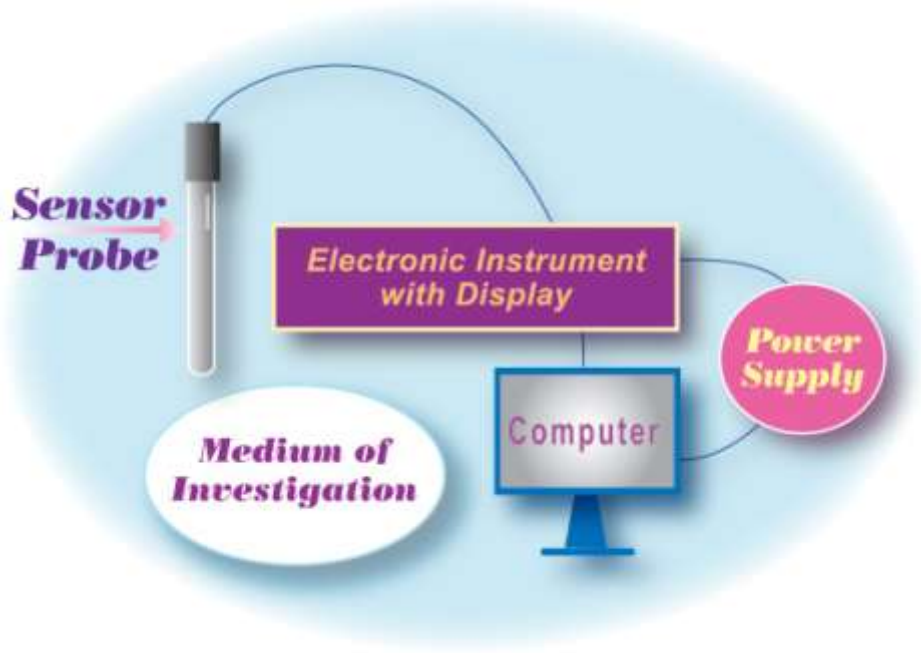

Figure 20. Diagram of our over-all experimental setup.

From Chemistry fundamentals, the pH is defined as in Equation 16

$$pH = -\log_{10}(a_{H^+}), \qquad (16)$$

where a is the chemical activity of the H^+-ion and $a_{H^+} = \gamma_{H^+} C_{H^+}$. Here, C_{H^+} is the actual concentration of $a=\gamma C$, the H^+ ion in the aqueous solution to be tested and γ_{H^+} is the thermodynamic activity coefficient for H^+ which is ~1.0 for dilute solutions. The C-effect is very localized while the γ-effect is long range (non-local). Although the dissociation of H_20 creates H^+-ions, the carbon dioxide, CO_2, in our air dissolves into the water to greatly increase the H^+-ion content and make the water acidic at a pH-value of approximately 5.6 rather than neutral at a pH of 7.0. A third important type of chemical reaction that occurs in our water/air system arises due to the presence of impurities like calcium, magnesium, etc, which dissolve into the water, ionize and convert HCO_3 ions to a carbonate particle plus an H^+-ion. These microscopic-sized carbonates grow in size and eventually settle to the bottom of the vessel as a precipitate. The commercial bottled water called Evian is a dilute calcium-magnesium bicarbonate solution that is oversaturated with CO_2 compared to the same water in equilibrium with local air. On opening an Evian bottle, this "excess" CO_2 leaves the water to the air so the H+-ion concentration slowly decreases over time and the water becomes more alkaline (the pH increases).

In our research, we highly purify the starting water to a pH = 7.0 which, when it is exposed to room air, CO_2 enters the water and reduces it to a pH ≈ 5.60 (more acidic). In this way, we always know the starting pH of our water and, in fact, can calculate a rigorous theoretical value for that starting pH for **all** of our IHD experiments.

The physical aspect of digital pH-measurement involves the use of a pH-electrode which connect s (1) a unit activity standard chemical cell to (ii) a water solution vessel whose H^+-activity is to be measured via (iii) an H^+-permeable membrane between (i) and (ii). As the H^+-ion redistributes itself in this system to produce electrochemical potential equilibrium for the H+-ion throughout the system, the H^+-ion distribution develops a profile like that shown in Figure 21(a).

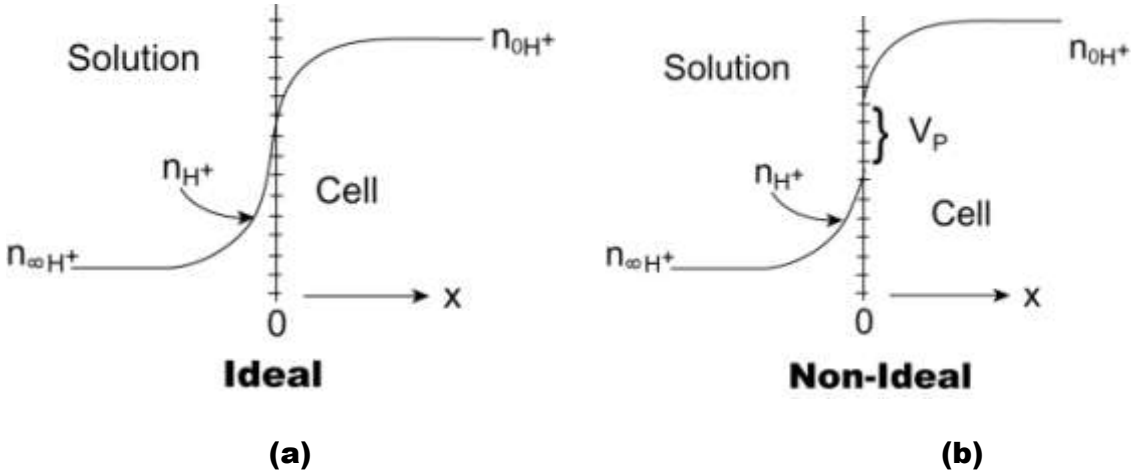

Figure 21. Plots of H^+ ion population density, n_{H^+}, profiles in a pH-electrode for (a) the ideal case and (b) the non-ideal case.

This thermodynamic equilibrium process is defined by the general Boltzmann equilibrium equation for H^+ which is mathematically expressed by

$$\frac{a_{H^+}}{a_{0H^+}} = exp\left[\frac{-|e|}{kT}\left\{V-\left(V_0+V_P\right)\right\}\right]. \qquad (17a)$$

Here, exp is the exponential function, V_0 is the electric voltage of the standard chemical cell in Figure 21a, $V_P = 0$ in this case, but is most generally non-zero, and is the interface polarization voltage (see Figure 21b) due to the redistribution of all other chemical species in the solution, V is the solution voltage, a_0 is chemical activity for the standard cell while $|e|/2.303\ kT = 59.16$ millivolts ($|e|$ is the proton charge, T is the absolute temperature and k is Boltzmann's constant). Combining Equations 16 and 17a with $a_{0H^+} = 1$, $V_P = 0$ and $\log_{10}(exp) = 1/2.303$, one obtains the simple relationship connecting the physical measurement, $V - V_0$, to the solution pH as

$V = V_0 - 59.16\ pH\ (mV)$. (17b)

For the **non-ideal** pH-electrode case, illustrated in Figure 21b, where V_P has a non-zero value, a commercial pH-meter's CPU incorporates a corrected temperature factor and uses the following **parametric** expression to display the pH from an internal measurement of V,

$$V = S\left(pH_{U(1)} - 7\right)T_{corr} \quad where\ T_{corr} = \frac{T + 273.15}{298.15} \ . \qquad (18a)$$

Here, S is the electrode slope = $d[V-(V_0+V_P)]/dpH$ and $pH = pH_{CPU} = pH_{(U(1))}$. In addition, V_0 is taken to be -7S, since the experimental isopotential point (V = 0) is found to occur at pH = 7 for an **ideal electrode**. In order to make these parametric choices of the commercial pH-electrode suppliers fit the fundamental physics implicit in Equation 17a, the following is also required for internal self-consistency

$V_P = (S + 59.16)\ pH_{U(1)}\ T_{corr}$. (18b)

One can take Equation 18a and define a new parameter, N, and call it **the Nernst Parameter**, in honor of that great physical chemist of the 1800's, where

$$N = \frac{S}{V}(pH - 7)T_{corr} \quad . \qquad (19)$$

Of course, N should equal unity for the U(1) state and experimental data shows that, for "unconditioned" spaces, N = 1 is observed. Back in ~January, 2003, early in our replication phase of the Minnesota ΔpH = +1 IHD work[14], Figure 22 illustrates a plot of N-value as a function of time derived from pH-values at Station 4 of the Payson-site (P_4) while Table 1 provides some N-values for a variety of different sites in our total experimental system of that time. Clearly, some space "conditioning" was taking place at some sites.

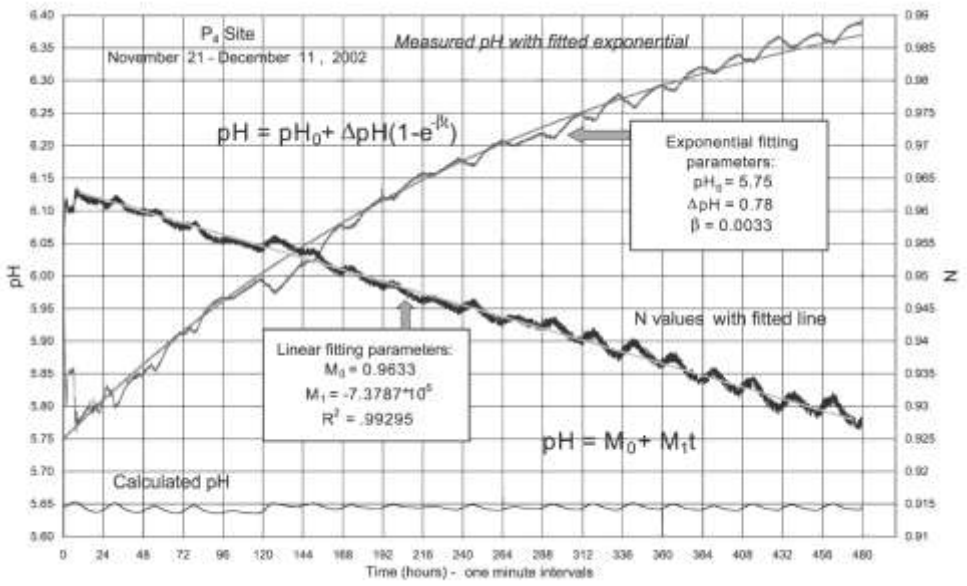

Figure 22. Showing the time-average exponential variation of pH and N after fresh purified water was introduced into the measurement cell on 11/21/02.

Table 1

Values of N for all of the various sites operating in our overall experimental system.

Site	Recent N-values	% departure from 1.00
P_1	.89	-11
P_2	1.14	14
P_3	.98	-2
P_4	.87	-13
M_1	1.3	30
K_1	.98	-2
B_2	1.23	23
B_1	1.04	4

In this Table, P=Payson, K=Kansas, M=Missouri, B_A=Baltimore and B_B=Bethesda and the subscript numbers stand for particular measurement stations located at these geographic sites (see Reference 14) as of ~January 25, 2003.

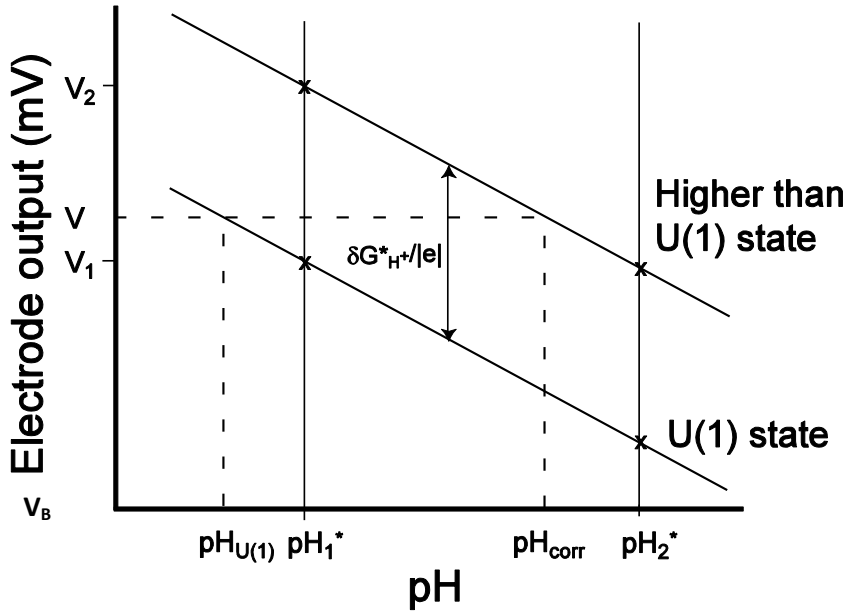

Figure 23. The electrode electrical output vs. pH plots for both the U(1) state ($\delta G^*=0$) and a higher than U(1) EM gauge symmetry state.

When the experimental space has been IHD-conditioned to a higher thermodynamic free energy state for the H+-ion by an amount $\delta G^*_{H^+}$, relative to the N = 1 state, the electrode vs. pH-plot, assuming the same slope as that for the U(1) gauge state, is given in Figure 23 and Equation 17a is altered to

$$\frac{a_{H^+}}{a_{oH^+}} = exp\left[\frac{-|e|}{kT}\left\{V - \left(V_o^* + V_p^*\right) + \frac{\delta G^*_{H^+}}{|e|}\right\}\right] \qquad (20a)$$

and

$$V = s\left(pH_{U(1)} - 7\right)T_{corr} - (1 + T_{corr}) + \frac{\delta G^*_{H^+}}{|e|} \qquad (20b)$$

where

$$T_{corr} = T + \frac{273.15}{298.15}. \qquad (20c)$$

At the experimental isopotential point for the pH-electrode, V = o, and thus, from Equation 20b, we obtain

$$\frac{\delta G^*_{H^+}}{|e|} = S\left(pH^o_{U(1)} - 7\right)\frac{T_{corr}}{1+T_{corr}}. \qquad (21)$$

Experimentally, one can determine the isopotential point, $pH^o_{U(1)}$, via the use of two or three buffer solutions if a linear relationship between V and $pH_{U(1)}$ is measured (as in Figure 24). Measurement of $pH^o_{U(1)}$ at nine different stations in the Payson laboratory, using the two-buffer solution standards procedure, was carried out with various electrodes (see Figure 24). These electrodes were all of the same commercial type, but had quite different use histories.

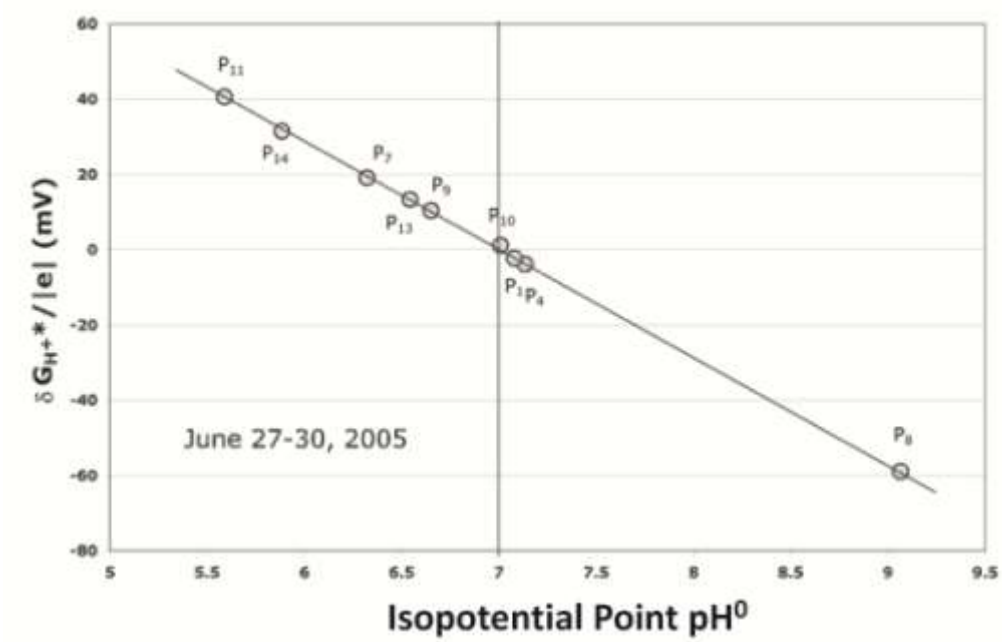

Figure 24. δG^*_H vs. isopotential point of various electrodes (same type) used at the various P_j stations shown (for the Payson laboratory at calibration). **The only difference between electrodes used at these stations is their history**. The type of space the electrode is exposed to causes the isopotential point to depart from 7.

Figure 24 is a beautiful linear plot, in complete accord with Equation 21, which yields $\delta G^*_{H^+}$ at $pH^o_{U(1)}$=7 as expected.

The important takeaway information from this section is that:

1. It is possible to calculate the **excess** thermodynamic free energy per unit volume, $\delta G^*_{H^+}$,in an IHD-conditioned space for the aqueous H^+-ion at a level very different than that for our conventional U(1) electromagnetic gauge symmetry state.

2. This digital pH-probe system provides great utility as a "subtle energy" sensor (tool) for quantitatively measuring the departure of a room from the thermodynamic free energy state of our normal, U(1) gauge state physical reality.

As one specific example to illustrate the use of our pH-measurement system as a subtle energy detector, we were asked by Dr. Eric Pearl of Reconnection Healing to come to one of their healing workshops and experimentally measure the subtle energy changes during the workshop events. One such workshop was in Los Angeles, CA in July 2007. We agreed to test our system at this venue and Figure 23 illustrates a meaningful schematic of the workshop room setup.

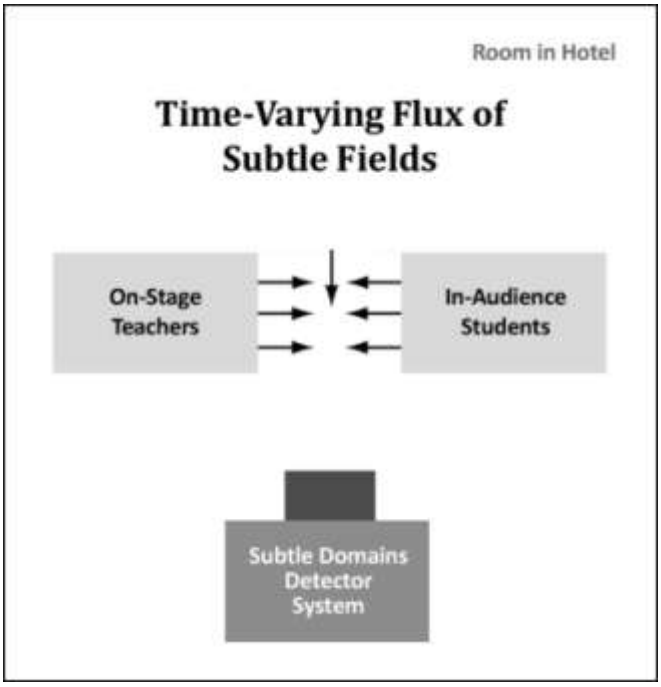

Figure 25. Schematic of the room setup for the Reconnection workshop.

Consistent pH changes were observed when people sat listening intently to the on-stage demonstration and instruction and then got up to move around. This is shown in Figure 24 using some of our pH results. In Figure 24 the pH changes were converted to the thermodynamic free energy quantity, $\delta G^{*}_{H^+}$. This quantity reflects how the energy changes (in milli electron volts) for a given change in pH. The importance of the Figure 24 data is that, **every time** the students sat down and paid attention to the onstage workshop teacher, the **magnitude** of $\delta G^{*}_{H^+}$, increased (more negative) and **every time** the students stood up and walked around, the magnitude **decreases** (less negative). We interpret these pH-changes as (1) the thermodynamic entropy decreases (because the information content increased) (2) increased entropy creation occurs when participants stand up to walk around and chat with each other. The net result of this information increase, (and thus entropy decrease) is that the overall

thermodynamic free energy per unit volume, G, of our **world** increases and it will last longer before it ultimately cools to the point that it will no longer support life as we know it. This is one **key purpose** for human existence and inner development.

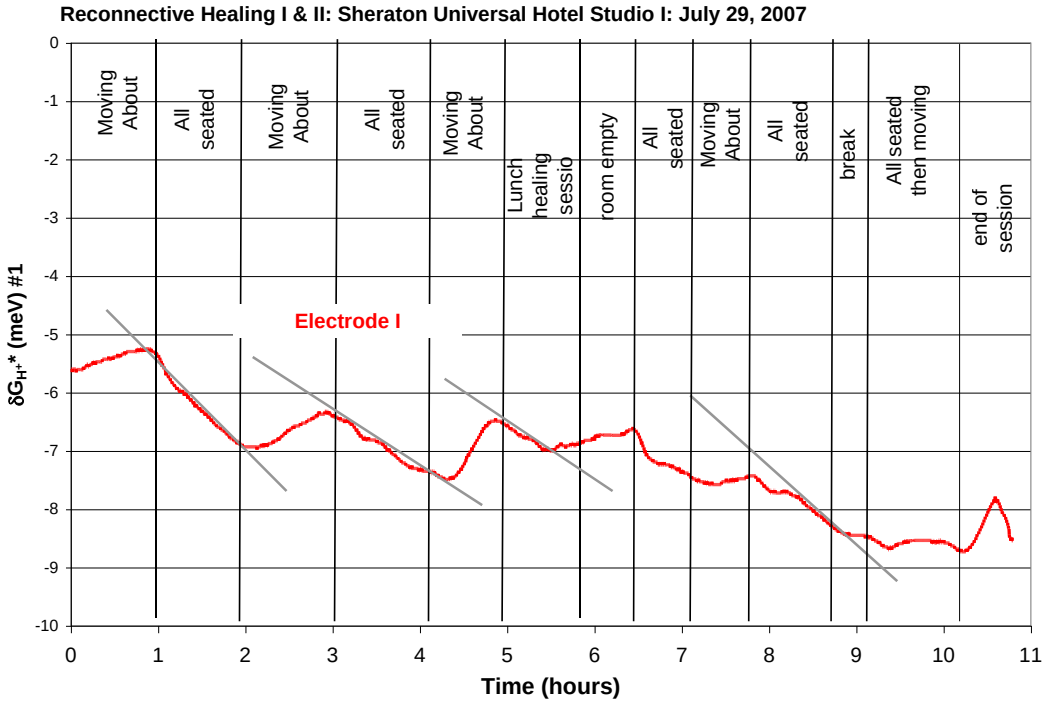

Figure 26. $\delta G^*_{H}+$ for the space vs. time.

References

1. W. A. Tiller, W. E. Dibble, Jr., and M. J. Kohane, Conscious Acts of Creation: The Emergence of a New Physics (Pavior Publishing, Walnut Creek, CA, USA, 2001).
2. W.A. Harrison, Applied Quantum Mechanics (World Scientific, Singapore, 2000).
3. R.M. Eisberg, Fundamentals of Modern Physics (John Wiley and Sons, Inc., New York, N.Y., 1961).
4. S.G. Lipson and H. Lipson, Optical Physics (Cambridge University Press, New York, N.Y., 1969) pp 34 and 310.
5. R. Bracewell, The Fourier Transform and its Application (McGraw-Hill Book Co., New York, N.Y., 1965).
6. G. Harburn, C.A. Taylor and T.R. Wellberry, Atlas of Optical Transforms (Cornell University Press, Ithica, N.Y., 1975).
7. K. Pribram, Brain and Perception, Holonomy and Structure in Figural Processing (Lawrence Erlbaum Associates, Hillsdale, N.J., 1991).
8. Microwave Scanning Antennas, ed. R.C. Hansen: Volume II, Array Theory and Practice (Academic Press, New York, N.Y., 1966).

9. P. Werbos, “What do neural nets and quantum theory tell us about mind and reality?”, in No Matter, Never Mind, eds. K. Yasue, M. Jiba and T.D. Senta (John Benjamins Publishing Co., Philadelphia PA, 2001).
10. W. A. Tiller, W. E. Dibble, Jr., and M. J. Kohane, Conscious Acts of Creation: The Emergence of a New Physics (Pavior Publishing, Walnut Creek, CA, USA, 2001), p 49.
11. W. A. Tiller, W. E. Dibble, Jr., and M. J. Kohane, Conscious Acts of Creation: The Emergence of a New Physics (Pavior Publishing, Walnut Creek, CA, USA, 2001), G’t Hooft, “Gauge theories of the forces between elementary particles”, Scientific American, 242, 6 (1980) 104. .
12. W. A. Tiller, W. E. Dibble, Jr., and M. J. Kohane, Conscious Acts of Creation: The Emergence of a New Physics (Pavior Publishing, Walnut Creek, CA, USA, 2001), K. Moriyasu, An Elementary Primer for Gauge Theory (World Scientific Publishing Co. Pte. Ltd., Singapore, 1983).
13. W. A. Tiller, W. E. Dibble, Jr., and M. J. Kohane, Conscious Acts of Creation: The Emergence of a New Physics (Pavior Publishing, Walnut Creek, CA, USA, 2001), I.J.R. Aitchison and A.J.G. Hey, Gauge Theories in Particle Physics (Adam Hilger Ltd., Bristol, 1982).
14. W.A. Tiller and W.E. Dibble, Jr., “Towards general experimentation and discovery in ‘conditioned’ laboratory spaces, Part V: Data on ten different sites using a robust new type of subtle energy detector”, The Journal of Alternative and Complementary Medicine, 13, (3) (2007).